J. Fluid Mech. (1996), vol. 327, pp. 35–72

Experimental assessment of fractal scale-similarity in turbulent flows. Part 1. One-dimensional intersections

By RICHARD D. FREDERIKSEN[1], WERNER J. A. DAHM[1] AND DAVID R. DOWLING[2]

[1] Department of Aerospace Engineering, The University of Michigan, Ann Arbor, MI 48109-2118, USA

[2] Department of Mechanical Engineering and Applied Mechanics, The University of Michigan, Ann Arbor, MI 48109-2125, USA

(Received 8 August 1995 and in revised form 22 May 1996)

Results are presented from an assessment of the applicability of fractal scale-similarity in the spatio–temporal structure of $Sc \gg 1$ conserved scalar fields $\zeta(\boldsymbol{x}, t)$ and scalar energy dissipation rate fields $\nabla\zeta \cdot \nabla\zeta(\boldsymbol{x}, t)$ in turbulent flows. Over 2 million spatial and temporal intersections were analysed from fully resolved three-dimensional (256^3) spatial measurements as well as fully resolved four-dimensional spatio–temporal measurements containing up to 3 million points. Statistical criteria were used to assess both deterministic and stochastic fractal scale-similarity and to differentiate between fractal and random sets. Results span the range of spatio–temporal scales from the scalar diffusion scales (λ_D, T_D) to the viscous diffusion scales (λ_ν, T_ν) and to the outer scales (δ, T_δ). Over this entire range of scales, slightly over 99.0% of all intersections with the scalar dissipation support geometry showed scale-similarity as fractal as stochastically self-similar fBm sets having the same record length. Dissipation values above the mean were found to have support dimension $D = 0.66$. The dissipation support dimension decreased sharply with increasing dissipation values. Virtually no intersections showed scaling as random as a random set with the same relative cover. In contrast, intersections with scalar isosurfaces showed scaling only approximately as fractal as a corresponding fBm set and only over the range of spatio–temporal scales between (λ_D, T_D) and (λ_ν, T_ν). On these inner scales the isosurface dimension was $D = 0.48$ and was largely independent of the isoscalar value. At larger scales, scalar isosurfaces showed no fractal scale-similarity. In contrast, isoscalar level crossing sets showed no fractal scale-similarity over any range of scales, even though the scalar dissipation support geometry for the same data is clearly fractal. These results were found to be unaffected by noise.

1. Introduction

Among the principal difficulties in modelling the structure and dynamics of fluid turbulence is the wide range of length and time scales over which variations occur. This is the case in the velocity field as well as in the concentration fields of dynamically passive conserved scalar quantities mixed by the flow. Attempts to simplify the description of these turbulence fields on the basis of dynamical self-similarity assumptions date back as far as Kolmogorov (1941), Taylor (1935) and Richardson (1920). In more recent times, a broad class of such self-similar dynamical processes, namely the multiplicative stretching and folding common to many nonlinear systems,

has arisen as a possible means to characterize turbulence fields. Such a multiplicative process would lead to fractal geometries and multifractal scalings in the associated turbulence fields, which in turn would allow scaling properties of these fields over a wide range of length and time scales to be reduced to just a few parameters, among them fractal dimensions. The mathematical basis for fractal and multifractal descriptions of turbulence fields has by now been quite widely developed (e.g. Mandelbrot 1974; Frisch, Sulem & Nelkin 1978; Grassberger 1983; Hentschel & Procaccia 1983; Benzi *et al.* 1984; Frisch & Parisi 1985; Halsey *et al.* 1986; Meneveau & Sreenivasan 1991), and new classes of turbulence models based on these methods have begun appearing. However, direct experimental evidence for the applicability of these concepts, even for the comparatively simple fractal scale similarity potentially relevant to various geometric constructs in turbulent flows, has been inconclusive (e.g. Sreenivasan & Meneveau 1986; Sreenivasan & Prasad 1989; Sreenivasan, Ramshankar & Meneveau 1989; Sreenivasan 1991; Meneveau & Sreenivasan 1991; Prasad & Sreenivasan 1990; Miller & Dimotakis 1991; Lane-Serff 1993).

In velocity and scalar fields in turbulent shear flows, there are two principal length-scale ranges to which such fractal descriptions might apply. The first spans from the local outer scale δ (the scale of the mean shear profile), which is largely determined by the boundary and initial conditions of the flow, to the local inner scale λ_ν (the viscous scale), which is the result of a local balance between strain and vorticity diffusion in the flow. Between δ and λ_ν, there is a range of scales that are generally believed to exhibit a statistical self-similarity that leads, among other things, to the familiar $k^{-5/3}$ power-law scaling in the energy spectrum. A second range of scales, in which a different self-similarity exists, is present in conserved scalar fields $\zeta(\boldsymbol{x}, t)$ when the scalar diffusivity D is much smaller than the vorticity diffusivity ν, namely when the Schmidt number $Sc \equiv \nu/D$ is large. In that case, the local strain-limited scalar diffusion scale is $\lambda_D = \lambda_\nu Sc^{-1/2}$, and there exists a self-similarity for scalar-fluctuation length scales between λ_ν and λ_D that leads, among other things, to the k^{-1} power-law scaling in the scalar energy spectrum (Batchelor 1959). The self-similarity in these two length-scale regimes, presumably produced by some underlying multiplicative process, suggests the possibility of a fractal description for the scaling properties of the velocity and scalar fields in turbulent flows.

The precise self-similarity among scales that forms the basis for fractal geometry often refers to the repetition of a specific multiplicative mapping over a range of scales. Many classical fractals, such as the Cantor set, are generated by such a purely self-similar mathematical process. In turbulent flows such a precisely repeated scale similarity appears unlikely. However the notion of fractal scaling as satisfying precise deterministic scale similarity extends to stochastic scale-similarity as well, such as in the fractional Brownian motion (fBm) set. In such cases, a class of mappings characterized by one or more parameters is repeatedly applied, with the parameters constrained to satisfy certain statistics (e.g. Mandelbrot 1983; Feder 1988). A stochastic scale-similar multiplicative process in turbulent flows appears plausible, and would in turn produce various fractal signatures in the velocity and conserved scalar fields. Among these are the geometric scaling properties of dynamically passive conserved scalar fields being mixed by the underlying turbulent flow.

Previous studies of the applicability of fractal scaling concepts to conserved scalar fields in turbulent flows have reached contradictory conclusions. Sreenivasan & Prasad (1989), Prasad & Sreenivasan (1990) and Lane-Serff (1993) have reported finding essentially similar fractal scaling in the geometry of isoscalar surface fields for large-Sc mixing in the far field of an axisymmetric turbulent jet. While Prasad and Sreenivasan

reported not finding any variation in fractal dimension with the choice of isoscalar threshold level (see their figures 10 and 14), Lane-Serff has suggested that the measured dimension depends on the isoscalar value. Miller & Dimotakis (1991) have also examined the geometry of isoscalar level crossings for $Sc \gg 1$ conserved scalar mixing in the far field of the turbulent jet, and find an effect of the choice of scalar threshold value on the results obtained, but conclude that their data show no evidence for the fractal scaling found by Sreenivasan & Prasad and Lane-Serff.

The main difference between the studies from which these apparently contradictory conclusions were reached is the dimensionality of the scalar field data. Both Sreenivasan & Prasad and Lane-Serff based their studies on spatial analyses of scalar isosurfaces obtained from two-dimensional spatial intersections through the scalar field. In contrast, Miller & Dimotakis based their study on analyses of scalar threshold crossings from one-dimensional single-point time-series data, one-dimensional spatial data, and mixed space–time diagrams. As will be seen below, results of the present study show that the apparently conflicting conclusions from these previous studies are largely attributable to the different types of intersections analysed.

This study presents results from an experimental assessment of the applicability of fractal scaling in turbulent flows by examining the scaling properties in conserved scalar field measurements. As in the studies cited above, the data analysed are from laboratory measurements of the $Sc \gg 1$ conserved scalar field in the far field of an axisymmetric turbulent jet. However while the previous studies were restricted to either one-dimensional temporal data, two-dimensional space–time data, or two-dimensional spatial data, the present assessment is based on fully resolved three-dimensional (spatial) data as in figure 1, as well as combined four-dimensional (spatio–temporal) data for the space- and time-varying small-scale structure of the scalar field $\zeta(\boldsymbol{x}, t)$. This allows analyses of three-dimensional spatial data and one-dimensional time-series data acquired simultaneously in the same experiment, and thus comparisons of the scaling properties of true scalar isosurface sets and simple isoscalar level crossing sets. The present focus is primarily on an assessment of the geometrical scaling properties in the length-scale regime between λ_ν and λ_D, though some of the results presented also examine the scale similarity at larger scales. In addition, since some previous studies suggest an effect of the choice of threshold value on the geometric scaling properties of isoscalar surfaces, this study presents results for a range of isoscalar values spanning a factor of 20 around the mean. The present study also examines the geometric scaling properties of scalar dissipation fields $\nabla\zeta \cdot \nabla\zeta(\boldsymbol{x}, t)$, such as in figures 1(*b*) and 1(*d*), for a similar range of dissipation thresholds around the mean. The scalar dissipation field is of greater interest than the scalar field itself in many problems, and since the dissipation fields are inherently concentrated on compact support geometries, they may be potentially less sensitive to the choice of threshold value.

Finally, whereas previous studies have attempted absolute judgments as to the applicability of fractal scaling from individual experimental data records, the present study recognizes that it is fundamentally impossible to declare any finite-length record as being fractal or non-fractal. Instead it is at most possible to judge whether it is 'as fractal as some known fractal set having the same record length'. Accordingly this study undertakes rigorous comparisons of the signatures of finite-length records from deterministic and stochastic fractal sets (irregular Cantor sets and fBm sets) with experimental data of the same record length. It uses local fractal dimension maps and the χ^2 statistical criterion to objectively assess the applicability of fractal scale similarity for characterizing finite-length spatial and temporal data records spanning various length and time scale ranges in turbulent scalar fields.

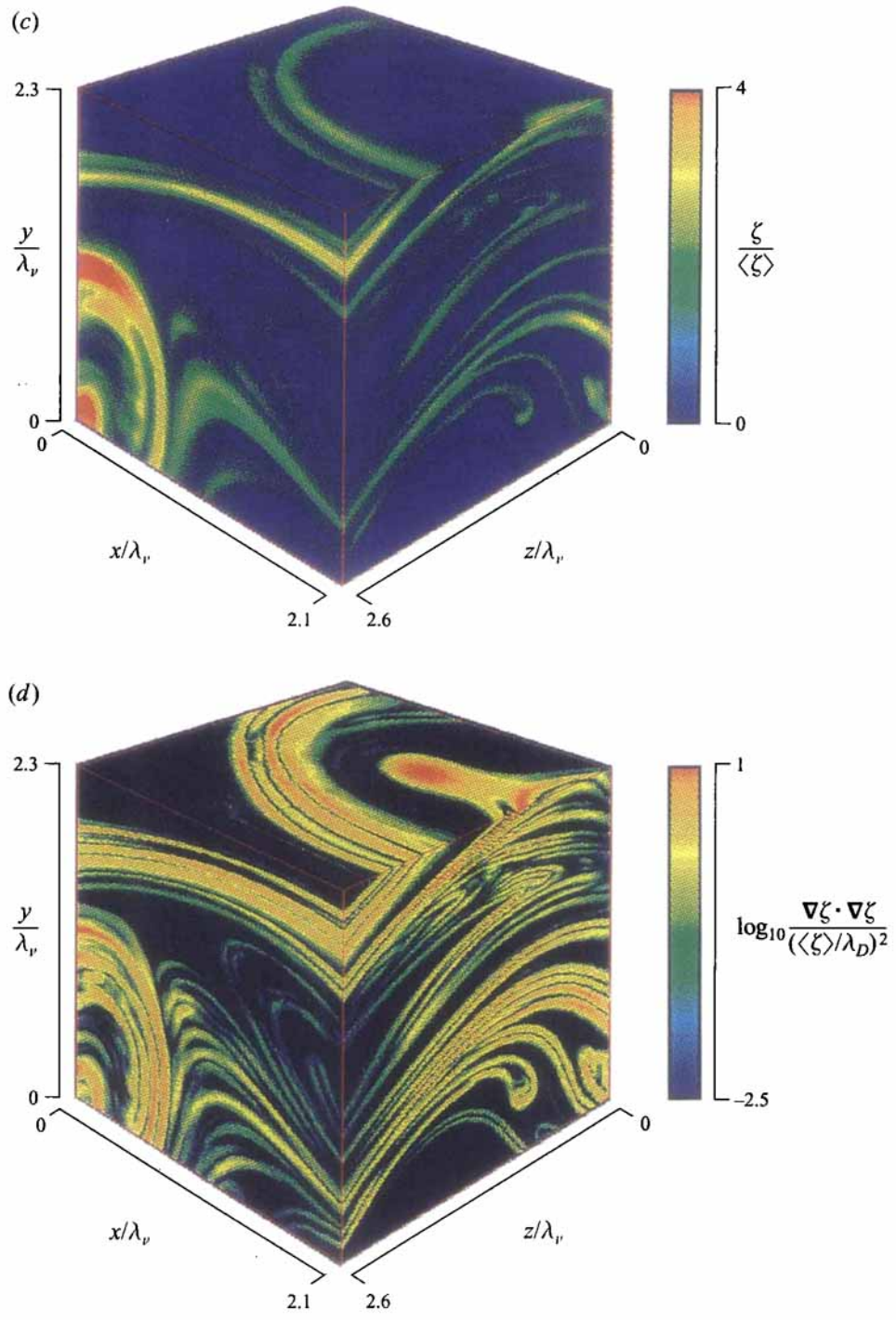

FIGURE 1(*a*, *b*). For caption see facing page.

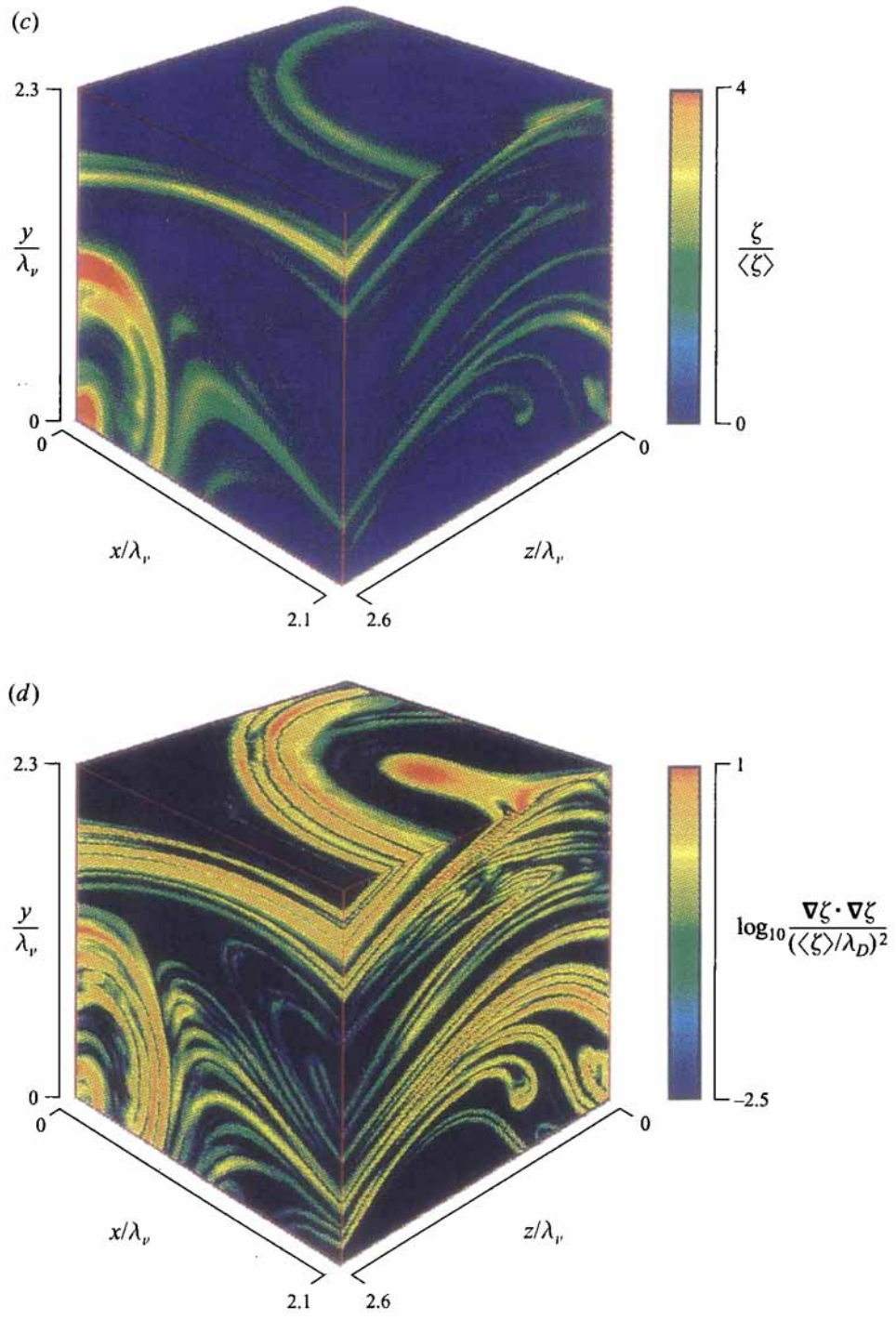

FIGURE 1. Examples of fully-resolved three-dimensional (256^3) spatial data volumes of the type analysed in the present study, showing the conserved scalar field $\zeta(\boldsymbol{x}, t)$ in (*a*, *c*) and the corresponding scalar energy dissipation rate field $\nabla\zeta\cdot\nabla\zeta(\boldsymbol{x}, t)$ in (*b*, *d*). Note the sheet-like structure of the dissipation support. Axes indicate scales relative to the local inner scale λ_ν of the underlying turbulent flow; $Re_\delta = 3700$, $Re_\lambda = 45$, $Sc = 2075$.

Data type	Re_δ	Re_λ	λ_D (μm)	λ_ν (μm)	$\Delta x, \Delta y$ (μm)	Δz (μm)	Beam (μm)
Three-dimensional (spatial)	3700	45	257	11700	109	120	181
Four-dimensional (spatio–temporal)	3000	41	303	13800	108	90	191

TABLE 1. The spatial resolution characteristics of the experimental data used in this study. For both the three-dimensional spatial data and four-dimensional spatio–temporal data the dimensions of the measurement volume ($\Delta x, \Delta y, \Delta z$) are less than half the molecular diffusion length scale λ_D.

Data type	Re_δ	Re_λ	λ_D/u (ms)	$\Delta\tau$ (ms)	Δt (ms)	ΔT (ms)
Three-dimensional (spatial)	3700	45	103	0.0238	8.87	2270
Four-dimensional (spatio–temporal)	3000	41	152	0.0238	8.87	53.2

TABLE 2. The temporal resolution characteristics of the experimental data used in this study. The pixel illumination time $\Delta\tau$ and data-plane acquisition time Δt for both the three-dimensional spatial data and four-dimensional spatio–temporal data are orders of magnitude smaller than the local scalar field advection time λ_D/u. Moreover, the time between acquisition of the same pixel in successive three-dimensional data volumes ΔT in the four-dimensional data is less than half the scalar field advection time. This, along with the spatial resolution of the data (see table 1), ensures that the data used in this study are fully resolved both spatially and temporally.

This paper, Part 1, presents results from analyses of scale similarity in one-dimensional spatial and temporal intersections through scalar isosurface fields and through scalar dissipation support fields. Part 2 (Frederiksen, Dahm & Dowling 1997*a*) gives corresponding results for higher-dimensional intersections through these fields, including evidence of non-fractal inclusions, and Part 3 (Frederiksen, Dahm & Dowling 1997*b*) assesses the applicability of multifractal scale similarity in conserved scalar fields and scalar dissipation rate fields in turbulent flows.

2. Data characteristics

The present results are obtained from analyses of laser-induced fluorescence data for $Sc \gg 1$ mixing in the self-similar far field of an axisymmetric turbulent jet in water. The measurement technique is described in detail in Dahm, Southerland & Buch (1991) and Southerland & Dahm (1994). Briefly, the concentration field $\zeta(\boldsymbol{x}, t)$ of a laser-fluorescent dye carried by the jet fluid was measured repeatedly in time at as many as 256^3 points within a small three-dimensional spatial volume located 235 diameters (1.15 m) downstream of the jet exit and 26 diameters (13 cm) off the jet centreline. A highly collimated laser beam was swept in a raster fashion through this volume, and the resulting laser-induced fluorescence from dye-containing fluid was imaged onto a high-speed, planar, 256 × 256 element, photodiode array. The array output was serially acquired at 8-bits true digital depth and continuously written in real time to a 3.1 GB high-speed parallel-transfer disk bank capable of accommodating more than 50000 such 256^2 data planes. The resulting measured fluorescence intensity field was subsequently converted to the true dye concentration as described in Southerland & Dahm (1994).

Each measurement produces the scalar field at over 3 billion individual points in space and time. To estimate the resulting spatial and temporal resolution for each of the cases

listed in tables 1 and 2, note that the local outer scale $\delta(x) \approx 0.44x$ and centreline velocity $u(x) \approx 7.2\,(J/\rho)^{1/2}\,x^{-1}$, with J the jet source momentum flux and ρ the ambient fluid density. For example, at the outer-scale Reynolds number $Re_\delta \equiv (u\delta/\nu) \approx 3700$ and with the Schmidt number of 2075, the local strain-limited estimate of molecular diffusion length scale is $\lambda_D \approx 257$ μm and the estimate of local advection time scale is $T_D \equiv \lambda_D/u \approx 103$ ms. For comparison, the in-plane spatial resolution was $\Delta(x, y) \approx 109$ μm. The (1/e) laser beam thickness was measured as 181 μm. Deconvolution of the scalar field measurements among adjacent planes increases the effective spatial resolution in the z-direction to the interplane separation $\Delta z \approx 120$ μm. These values show that both the characteristic scale of the pixel image volume $(\Delta x\,\Delta y\,\Delta z)^{1/3}$ and its maximum dimension (Δz) are less than $0.5\,\lambda_D$. Similarly, the temporal separation between successive data planes was $\Delta t = 8.9$ ms, and comparing with the diffusion-scale advection time of 103 ms verifies that the present measurements resolve essentially all of the fine-scale structure of the local turbulent mixing process.

In terms of classical Kolmogorov variables, the strain-limited molecular diffusion length scale $\lambda_D \approx \lambda_\nu Sc^{-1/2}$, where λ_ν is the local strain-limited viscous diffusion scale, and $\lambda_\nu \approx 5.9\,\lambda_K$ (Southerland & Dahm 1994) and $\lambda_K \equiv (\nu^3/\epsilon)^{1/4}$ is the Kolmogorov scale. Thus λ_ν is proportional to the Kolmogorov scale, but gives the average physical length scale of the finest vortical structures, with λ_D in turn proportional to the classical Batchelor scale but giving the physical length scale of the finest scalar gradient structures. In the four-dimensional data, the intervolume time of 0.05 s in all cases corresponds to less than half the scalar diffusion-scale advection time λ_D/u and thus less than 1/200 of the classical Kolmogorov time scale $(\nu/\epsilon)^{1/2}$. Similarly, in both the three- and four-dimensional data, the interplane time is 0.009 s, which even in the worst case is less than $(1/11)\,\lambda_D/u$, and thus is entirely trivial in terms of the Kolmogorov time. Consequently, the data acquisition rate is sufficient to effectively freeze the scalar field, and to entirely freeze the underlying velocity field.

The high spatial and temporal resolution achieved, together with the high signal quality attained, allows accurate differentiation of the measured conserved scalar field in all three spatial dimensions and in time. This makes it possible to determine the components of the true local instantaneous scalar gradient vector field $\nabla\zeta(\boldsymbol{x}, t)$ throughout these three- and four-dimensional data, without any need to resort to various approximations based on Taylor's hypothesis as is commonly required. This in turn permits determination of the true scalar energy dissipation rate field $\nabla\zeta \cdot \nabla\zeta(\boldsymbol{x}, t)$, and thus an assessment of the geometric scaling properties of the highly compact support on which this field is concentrated in turbulent shear flows.

Similarly, the temporal separation between adjacent data planes within each three-dimensional (256^3) spatial data volume, and between the same data point in successive spatial volumes with fewer z-planes in the fully four-dimensional data, is shorter that the local diffusion-scale advection time T_D. As a result it is possible to extract fully resolved time-series data of the type shown in figure 2 from both the conserved scalar field $\zeta(\boldsymbol{x}, t)$ and scalar energy dissipation rate field $\nabla\zeta \cdot \nabla\zeta(\boldsymbol{x}, t)$, again without invoking any of various classical approximations. This in turn permits direct comparisons between geometric scaling results from multi-dimensional spatial data and one-dimensional time-series data, both obtained from the same realization of the conserved scalar field.

Finally, note that the imaged region in the turbulent scalar field in these experiments typically spans less than 1/15 of the local outer scale δ, and is comparable to the local inner scale λ_ν of the flow. The structure of velocity and scalar fields in turbulent shear flows at scales near and below λ_ν is generally believed to be statistically universal. This

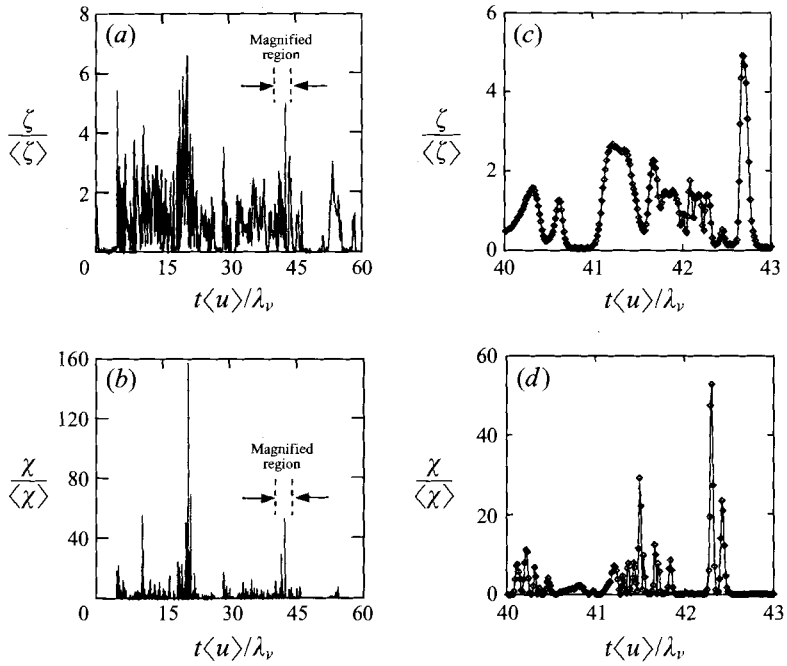

FIGURE 2. Examples from fully resolved four-dimensional spatio–temporal data of the type analysed in the present study, showing the time-variations in conserved scalar values $\zeta(a, c)$ and scalar dissipation values $\chi \equiv \nabla\zeta\cdot\nabla\zeta$ (b, d) at one spatial location from successively measured spatial data volumes. The entire duration of the measurement is shown (a, b), as well as a magnified section demonstrating the high temporal resolution achieved (c, d). Symbols show the discrete measured values.

contention appears to be true even for the present moderate Reynolds number flows, as evidenced by the measured collapse of small-scale spectra at similar Reynolds numbers by Dowling (1991), and by the DNS studies of Jiménez *et al.* (1993). The estimated Taylor-scale Reynolds numbers for the present data are $Re_\lambda \approx 45$, well within the range of values over which the DNS results of Jiménez *et al.* showed Reynolds-number-independent collapse on inner variables at the smallest flow scales. Moreover, high-wavenumber spatial scalar spectra from these same data (Southerland, Dahm & Dowling 1995) show the k^{-1} scaling predicted by Batchelor for large-Sc mixing in turbulent flows. As a result, even though the present measurments are from $Re_\delta \approx 3500$ turbulent jets, the geometric scaling properties of the fine scales derived from them are believed to be largely representative of the generic scaling properties at the inner scales of all turbulent shear flows.

3. Box counting criterion

There are numerous methods for determining fractal scaling and dimension from experimental data. These range from box counting schemes to methods based on spectra and correlation techniques (Dubuc *et al.* 1989; Theiler 1990), and for sufficiently long record lengths many techniques can be satisfactorily applied. However in the present study, the three-dimensional (256^3) spatial data volumes and four-dimensional spatio–temporal data produce record lengths of only 256 points in any spatial direction and 4096 points in the temporal direction. These relatively short

record lengths required techniques for accurate determination of scale similarity properties. Two related methods were developed based on a box counting algorithm and a χ^2 probability test to objectively determine if a given set of records follow fractal scaling. These methods give accurate results for numerically generated fractal and non-fractal records having lengths commensurate with the present experimental data.

The record being analysed is first covered with a grid of boxes of a fixed size (ϵ/L), where L is the record length, and the number N of boxes that contain any portion of the set is counted. The variation in N with scale (ϵ/L) determines the geometric scaling properties of the set. In particular, a linear relation between $\log N$ and $\log(\epsilon/L)$ for small (ϵ/L) indicates power-law (fractal) scaling of the form $N \sim (\epsilon/L)^{-D}$, with the fractal dimension D determined by the slope. This widely used approach is motivated by the definition of the fractal dimension, namely

$$D \equiv \lim_{(\epsilon/L)\to 0} -\frac{\mathrm{d}\log(N)}{\mathrm{d}\log(\epsilon/L)}, \tag{1}$$

where, if the limit exists, the set is fractal and the limit value is its fractal dimension D.

However, the limit in (1) cannot be accurately approximated with short record lengths. For this reason, over the accessible range of scales the present box counting method instead looks for an asymptotic approach to scaling of this type in what is often termed the 'local fractal dimension' $D(\epsilon)$, given by

$$D(\epsilon) = -\frac{\mathrm{d}\log(N)}{\mathrm{d}\log(\epsilon/L)}. \tag{2}$$

This is demonstrated in figure 3, where $N(\epsilon)$ results from irregular Cantor sets with relatively long record lengths (2^{18} points) and dimensions $D = \{0.2, 0.45, 0.64, 0.84\}$ are shown in figure 3(*a*), together with the associated $D(\epsilon)$ in figure 3(*b*) resulting from linear central differences on $N(\epsilon)$ to approximate the derivative in (2). Although the $N(\epsilon)$ results in figure 3(*a*) appear nominally linear for small (ϵ/L) in the logarithmic axes shown, the more sensitive test in figure 3(*b*) reveals significant departures from the constant $D(\epsilon)$ that would confirm true fractal scaling. As the box size $(\epsilon/L) \to 0$, the $D(\epsilon)$ results asymptote toward constant values; however, with decreasing D this approach becomes quite slow (since N becomes relatively small) and requires increasingly longer record lengths. For any finite record composed of p equally spaced discrete points, the smallest accessible box size is $(\epsilon/L) = 1/p$. With the 256-point records from the present spatial data, our $D(\epsilon)$ results are thus confined to $2 \leqslant -\log_2(\epsilon/L) \leqslant 7$. This accessible range of scales in figure 3(*b*) is separated into two regions (Regions 1 and 2), the former dominated by the decrease in $D(\epsilon)$ at relatively large box sizes, and the latter in which an asymptotic approach to constant $D(\epsilon)$ becomes evident for the higher dimension cases. The standard deviation σ in the average $D(\epsilon)$ of each individual record over Region 2 in figure 3(*b*) depends on the true dimension D, and provides a means for assessing the asymptotic approach in (1) and determining the true dimension.

The criterion for declaring an ensemble of finite-length records as being fractal then becomes that the ensemble of $D(\epsilon)$ values from (2) over a selected range of scales (ϵ/L) must have the same statistics as the values generated over the same range of scales by an ensemble of true fractal sets having the same record length and dimension $D = \langle D(\epsilon)\rangle$. The records in the ensemble are then 'as fractal as the true fractal is over the accessible range of scales'. In practice this criterion is satisfied if the variances of both distributions are equal.

To establish the criterion $\sigma(\langle D(\epsilon)\rangle)$ against which the geometric scaling properties

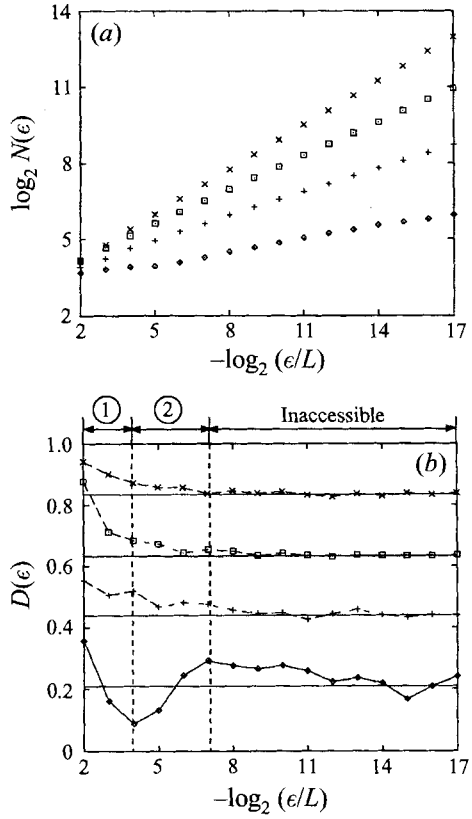

FIGURE 3. Box counting results for individual realizations of irregular Cantor sets with $D = \{0.20, 0.45, 0.64, 0.84\}$, showing $\log_2 N(\epsilon)$ (*a*) and corresponding local dimensions $D(\epsilon)$ obtained by linear central differencing (*b*). Note the effect of dimension and record length on convergence of $D(\epsilon)$ to D.

of the experimental records are compared, (2) was applied to 10000 numerically generated irregular Cantor sets for each of several fractal dimensions D. Irregular Cantor sets are generated from a unit line segment as the initiator, and a generator consisting of a set of distinct line segments of lengths $[c_1, c_2, \ldots, c_m]$. which form a subset of the initiator. At each stage of the construction every line segment of the initiator is replaced by a properly scaled version of the generator. This process is repeated until the desired resolution is reached. The fractal dimension of the resulting irregular Cantor set is given by

$$\sum_{i=1}^{m} (c_i)^D = 1. \tag{3}$$

The classical 'middle-third' Cantor set corresponds to $c_1 = c_2 = 1/3$, giving the fractal dimension $D = 0.631\ldots$. However the use of irregular Cantor sets allows many different realizations with the same fractal dimension. Figure 4(*a*) shows the results for $N(\epsilon)$ obtained from 10000 256-point record lengths irregular Cantor sets with $D = 0.5$, with the corresponding $D(\epsilon)$ values shown in figure 4(*b*). Over the range of scales $4 \leqslant \log_2(\epsilon/L) \leqslant 7$, these give $\langle D(\epsilon)\rangle = 0.536$ and $\sigma = 0.020$.

For precisely self-similar fractals like the irregular Cantor sets in figure 4, the resulting σ values are small (see table 3), which produces a very strict requirement for judging any 256-point record to be 'as fractal as a Cantor set'. However, since any repeated multiplicative mapping in turbulent flows is likely to be at most statistically

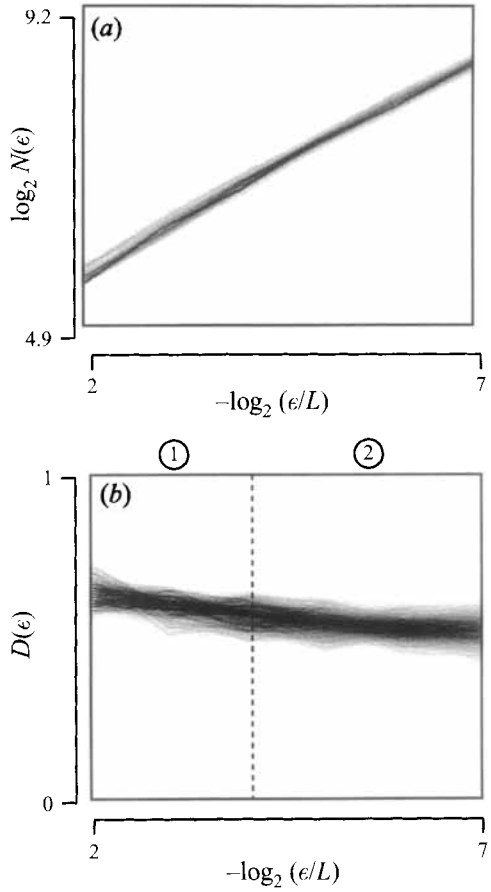

FIGURE 4. Box counting results for 10000 realizations of deterministically self-similar irregular Cantor sets with $D = 0.5$ and 256-point record lengths, showing relative densities in $\log_2 N(\epsilon)$ (*a*) and the local dimension $D(\epsilon)$ (*b*). Compare with stochastically self-similar fractal sets in figure 5.

	Cantor sets		fBm sets	
D	$\langle D \rangle$	$\sigma(\langle D \rangle)$	$\langle D \rangle$	$\sigma(\langle D \rangle)$
0.1	0.222	0.029	0.137	0.128
0.2	0.237	0.038	0.205	0.138
0.3	0.330	0.052	0.291	0.134
0.4	0.444	0.028	0.381	0.118
0.5	0.536	0.020	0.476	0.097
0.6	0.630	0.015	0.565	0.081
0.7	0.724	0.010	0.658	0.067
0.8	0.821	0.008	0.760	0.059
0.9	0.920	0.004	0.869	0.043

TABLE 3. $D(\epsilon)$ statistics from box counting analyses of 10000 irregular Cantor sets and fBm sets at each of nine different fractal dimensions D.

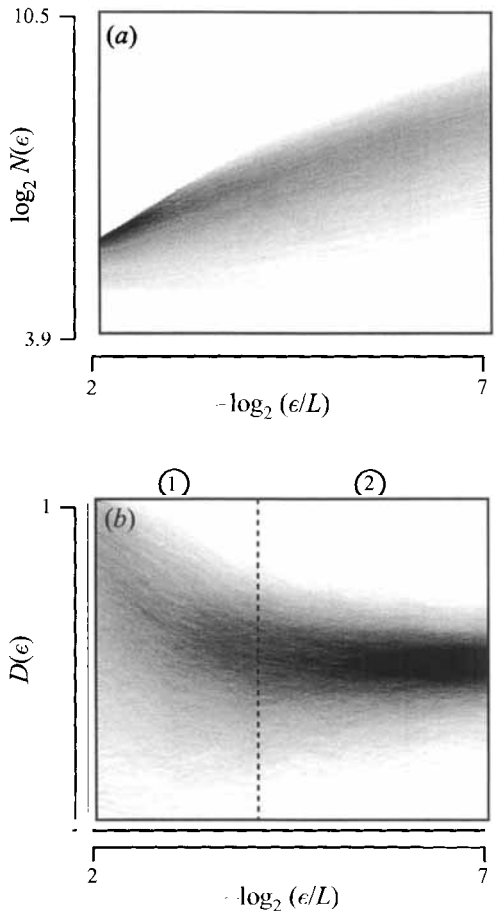

FIGURE 5. Box counting results for 10000 realizations of stochastically self-similar fBm sets with $D = 0.5$ and 256-point record lengths, showing relative densities in $\log_2 N(\epsilon)$ (*a*) and the local dimension $D(\epsilon)$ (*b*). Compare with deterministically self-similar fractal sets in figure 4, and with analogous results for 4096-point record lengths in figure 15.

self-similar, Cantor sets yield criteria for judging a turbulent scalar field record to be fractal that may be too strict. For this reason, analogous tests were performed with a class of statistically self-similar fractals, namely the level crossing sets produced by fractional Brownian motion (fBm) (e.g. Feder 1988). Figure 5 shows the $D(\epsilon)$ signature obtained from 10000 realizations of such fBm sets, each with the same dimension $D = 0.5$. Table 3 summarizes the results for fBm sets with fractal dimensions from 0.1 to 0.9, where the $\sigma(\langle D(\epsilon)\rangle)$ can be used to judge if any 256-point record can be declared to be 'as fractal as an fBm set having the same record length'.

4. χ^2 probability criterion

The approach to constant $D(\epsilon)$ in (2) can also be quantified in the $N(\epsilon)$ scaling itself by examining the linearity of $\log(N)$ with $\log(\epsilon/L)$ for each individual record. However, the inherently monotonic decrease in $\log(N)$ *vs.* $\log(\epsilon/L)$, even for non-fractal records, demands a strict criterion for discerning linearity. Classical statistics (Bevington & Robinson 1992; Press *et al.* 1992) provides a rigorous means to assess the

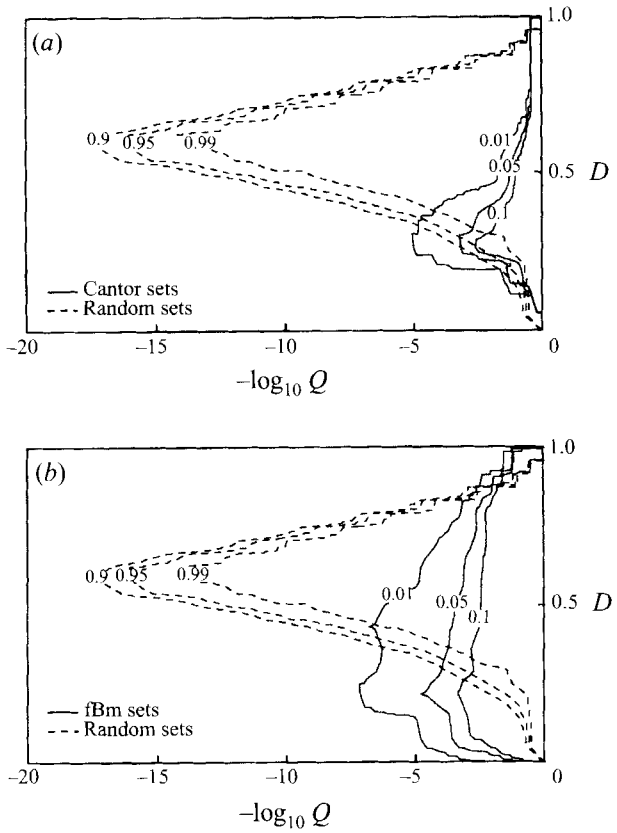

FIGURE 6. Cumulative probability contours of joint Q and $\langle D(\epsilon)\rangle$ values from each of the Cantor sets (*a*) and fBm sets (*b*) represented in table 3. Also shown are analogous contours for random sets having the same relative cover.

statistical significance of a linear least-squares fit to the $\log(N)$ *vs.* $\log(\epsilon/L)$ results for any record. This was accomplished with the χ^2 goodness-of-fit parameter

$$Q \equiv 1 - P\left(\frac{n-2}{2}; \frac{n}{2}\chi^2\right), \tag{4}$$

where P is the incomplete gamma-function, n is the number of points in the $\log(N)$ *vs.* $\log(\epsilon/L)$ data, and χ^2 is the mean-squared deviation from a linear fit normalized by the variances σ^2 obtained from an ensemble of true fractals. If the parameter Q is sufficiently large, then a linear fit as good as that obtained could not consistently occur by chance. Computing the Q value for any record and comparing it to a properly chosen threshold produces a criterion for evaluating each individual intersection for fractal scale similarity.

The threshold Q values for statistically declaring whether a given record is as fractal as various known fractal sets for the same record length were obtained by applying this criterion to irregular Cantor sets and fBm sets with the same dimension, and to randomly generated sets with the same relative cover. Results are presented in figure 6, where joint cumulative distributions of $\langle D\rangle$ and Q values for 10000 individual 256-point realizations of irregular Cantor sets (figure 6*a*) and of fBm sets (figure 6*b*) are shown for true dimensions D between 0 and 1. Also shown are results for 10000 random sets with 256-point record lengths and the same relative cover. The contours

show the boundaries within which a given fraction of the records lie. For instance, in figures 6(*a*) and 6(*b*) just 1% of all the fractal cases produce $\langle D \rangle$ and Q values to the left of the 0.01 contour, 5% of the fractal cases give values to the left of the 0.05 contour, etc. Similarly, 99% of the random sets produce values to the left of 0.99 contour, 95% of the random cases produce values to the left of 0.95 contour, etc. Comparing figures 6(*a*) and 6(*b*) shows that the statistically self-similar fBm fractal sets produce lower Q values than do the precisely self-similar irregular Cantor sets. However, even for the fBm sets, there is a clear separation between the Q values obtained from fractal and random sets (except at very large and very small dimensions).

This effectively allows any individual 256-point record from the experimental data to be judged as fractal as an fBm set, or possibly even as fractal as a Cantor set. The $\langle D \rangle$ and Q values obtained for each record correspond to a single point in each of figures 6(*a*) and 6(*b*). For an ensemble of such records, the corresponding joint $\langle D \rangle$ and Q probability densities allow identification of the percentage of records that are as fractal as any given percentage of the fractal test cases, or as random as any given percentage of the random test cases. In practice, we examine the fraction of records that fall to the right of the 0.01 contours in figures 6(*a*) and 6(*b*) to determine the percentage of records that are as fractal as 99% of the fractal test cases.

Lastly, mention must be made of the possible effects of any cutoff in the range of scales over which fractal scalar similarity might occur. The fBm and Cantor sets used here as test fractals are uniformly scale-similar at all scales. In the experimental data there is the possibility of a break in the scaling, or even a cutoff in the scaling range, near the diffusive scales λ_v and λ_D. Given the relatively short record lengths used in this study, it is not possible to test for such effects, and thus the criteria described above provide a comparatively stringent test for uniform scale-similarity over the entire range of scales investigated.

5. Effects of noise

To ensure that any assessment of the scale-similarities in experimental data is not strongly influenced by noise effects, it is necessary to either attempt to remove noise in the data by filtering, or else to show that its effects on the analyses are negligible. The former approach was taken by Miller & Dimotakis (1991), who attempted to remove noise by applying an optimal Wiener filter. Their results, however, showed that filtering can have a potentially significant effect on results from box counting analyses. Accordingly, the data in the present study were not filtered so as to prevent any loss of information or possible filter signature imprinting. Instead, the sensitivity of the results to synthetically generated noise was investigated.

This was done by adding Gaussian noise at levels up to ten times the expected noise in the measurements to the scalar field data, and then using the noise-enhanced data to produce scalar isosurface fields and scalar dissipation fields. Statistics from these noise-enhanced fields were then used to modify both fractal and non-fractal test cases of the type in the previous sections. Results showed that, even at ten times the expected noise level, there was less than a 2% change in the number of sets determined to be fractal and non-fractal. Moreover, with increasing simulated noise there was only a slight increase in the average dimension estimate $\langle D(\epsilon) \rangle$ of the fractal sets. These results are summarized in figure 7, and give a clear indication that experimental noise in these data was not an obstacle in the present assessment of fractal scale-similarity.

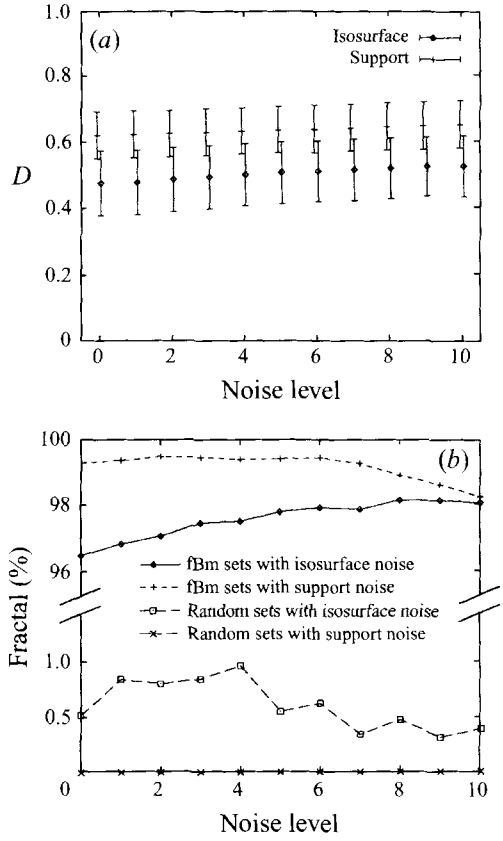

FIGURE 7. Effects of noise on box counting results for scalar isosurface sets and dissipation support sets, showing the insensitivity to noise in $\langle D(\epsilon)\rangle$ and σ (*a*), and in the fraction of fBm sets and random sets judged to be fractal (*b*).

6. Results for 256-point spatial intersections

Over 2 million individual one-dimensional spatial intersections through three-dimensional (256^3) data volumes of the type shown in figure 1 were analysed using the fractal assessment criteria described above. The scaling properties of the mean scalar isosurface geometry in conserved scalar field data $\zeta(\boldsymbol{x}, t)$ of the type in figure 1(*a*, *c*) were examined, as were the properties of the dissipation support geometry on which scalar energy dissipation rate fields $\nabla\zeta\cdot\nabla\zeta(\boldsymbol{x}, t)$ of the type in figure 1(*b*, *d*) are concentrated.

6.1. *Scalar dissipation support geometry*

The support set on which the scalar dissipation field $\nabla\zeta\cdot\nabla\zeta(\boldsymbol{x}, t)$ is concentrated consists of all spatio–temporal points where the dissipation lies above a selected threshold value. For the results in this subsection, this threshold was chosen at the mean dissipation value; effects of varying the threshold value are examined in §7. The resulting scaling properties of the dissipation support-set geometry are presented in figure 8, and represent ensemble statistics collected from over 2 million one-dimensional 256-point spatial intersections through the true three-dimensional dissipation field over the range of scales between the scalar diffusion scale λ_D and the viscous diffusion scale λ_ν.

Figure 8(*a*) gives the ensemble $D(\epsilon)$ results, where the average dimension obtained

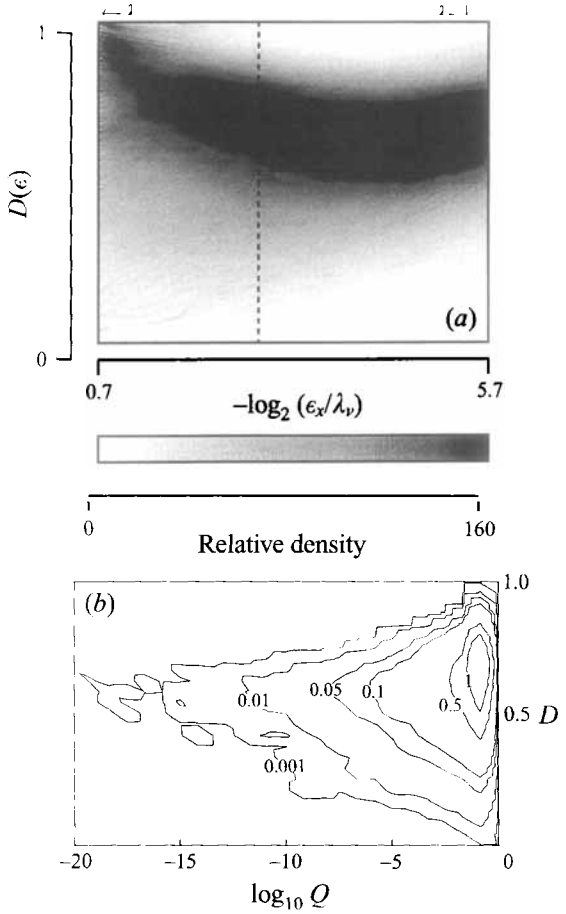

FIGURE 8. Spatial scale-similarity results for the dissipation support geometry at the inner scales $\lambda_D \leqslant \epsilon_x \leqslant \lambda_v$, showing $D(\epsilon)$ signature (*a*) and joint Q and $\langle D(\epsilon)\rangle$ signature (*b*). Compare with figures 10 and 18. Data are from over 2 million 256-point spatial intersections through scalar energy dissipation fields $\nabla\zeta\cdot\nabla\zeta(x, t)$ in three-dimensional (256^3) data volumes of the type in figure 1(*b*).

in Region 2 is $\langle D\rangle = 0.619$. It is apparent that the local dimension signature $D(\epsilon)$ at length scales ϵ between the viscous and scalar diffusion scales is fundamentally different from that in figure 4(*b*) for 256-point irregular Cantor sets with a single dimension. From this it can be firmly concluded that the dissipation support geometry at the inner scales of turbulent flows is definitely not as fractal as a Cantor set having a single dimension. However the $D(\epsilon)$ results in figure 8(*a*) do strikingly resemble the signature in figure 5(*b*) for 256-point fBm sets. Indeed, the standard deviation of $D(\epsilon)$ in Region 2 in figure 8(*a*) is $\sigma = 0.137$. This should be compared with the $\sigma = 0.015$ value in table 3 for irregular Cantor sets having the same average dimension $\langle D\rangle$ of 0.619, and with $\sigma = 0.074$ for fBm sets with $\langle D\rangle = 0.619$. Table 3 also shows that, for 256-point intersections through sets with scale similarity comparable to that of fBm sets, the average dimension estimate of 0.619 above corresponds to a true average dimension (at infinite record length) of $D = 0.658$.

Figure 8(*b*) gives the corresponding ensemble joint distribution of $\langle D\rangle$ and Q values for the dissipation support geometry. This should be compared with the probability contours for the corresponding irregular Cantor sets and random sets in figure 6(*a*), and for fBm sets and random sets in figure 6(*b*). Note that the precisely deterministic

scale similarity in the Cantor sets leads to much higher Q values than are demonstrated by the dissipation support set. However the stochastic scale similarity in the fBm sets produces Q values more in accordance with those in the dissipation support. In particular, 89.6% of the $\langle D \rangle$ and Q values in figure 8(*b*) are to the right of the contour bounding 99% of the fBm sets in figure 6(*b*), and only 1.3% are to the left of the contour bounding 99% of the random sets. Less than 10% of the intersections produced $\langle D \rangle$ and Q values that were between these two contours, and thus could not be judged to be as fractal as an fBm set having the same record length or as random as a random set with the same record length.

It must be concluded that 256-point intersections through the support geometry on which the scalar energy dissipation field is concentrated at the inner scales of turbulent flows follow scale similarity characteristics that, while they are not nearly as fractal as the deterministically self-similar Cantor sets, are nearly as fractal as the stochastically self-similar fBm sets. The somewhat larger σ in figure 8(*a*) may, however, be potentially indicative of at least a small variation in the dimension D of the dissipation support over this range of length scales.

6.2. *Scalar isosurface geometry*

Analogous results for the geometry associated with scalar isosurface crossings, obtained from over 2 million one-dimensional 256-point spatial intersections through the conserved scalar field $\zeta(\boldsymbol{x}, t)$, are given in figure 9. Ensemble statistics of the local fractal dimension $D(\epsilon)$ at length scales ϵ between the viscous and scalar diffusion scales are given in figure 9(*a*), where the average dimension obtained in Region 2 is $\langle D \rangle = 0.460$. Figure 9(*a*) should be compared with the corresponding signatures of 256-point Cantor and fBm sets in figures 4(*b*) and 5(*b*). As was the case for the dissipation support geometry, the precisely deterministic scale similarity in irregular Cantor sets such as in figure 4(*b*) leads to a much lower variation ($\sigma = 0.027$) in local fractal dimensions for the same average dimension than is found from the 256-point intersections through the scalar isosurface geometry ($\sigma = 0.122$) in figure 9(*a*). It can be concluded that the scalar isosurface geometry at the inner scales of turbulent flows is not nearly as fractal as a Cantor set with a single dimension. The measured σ value is much more consistent with the results for 256-point fBm sets of the type in figure 5(*b*), for which table 3 shows $\sigma = 0.101$ at the same average dimension $\langle D \rangle = 0.460$. Note also that table 3 indicates a true average dimension (at infinite record length) of $D = 0.48$ for sets showing scale similarity comparable to fBm sets with average dimension estimate of 0.619 for 256-point intersections. However, unlike the corresponding $D(\epsilon)$ map in Region 2 for an fBm set, figure 9(*a*) does not appear to asymptote to a strictly constant value indicative of true fractal scaling. This should be compared with the asymptotically constant $D(\epsilon)$ signature obtained in figure 8(*a*) for the dissipation support geometry over the same range of length scales from precisely the same data.

Consistent with this, the corresponding ensemble distribution of joint $\langle D \rangle$ and Q values for the spatial scalar isosurface geometry is given in figure 9(*b*). This should be compared with the probability contours for irregular Cantor sets, fBm sets, and random sets in figure 6. As was the case for the dissipation support geometry, the precise scale similarity in the Cantor sets in figure 6(*a*) leads to much higher Q values than are found in the scalar isosurface geometry. The stochastically self-similar fBm sets yield lower Q values that are more in accordance with those found from the scalar isosurface data. However, even though only 2.7% of the over 2 million intersections produced $\langle D \rangle$ and Q values to the left of the contour bounding 99% of random sets,

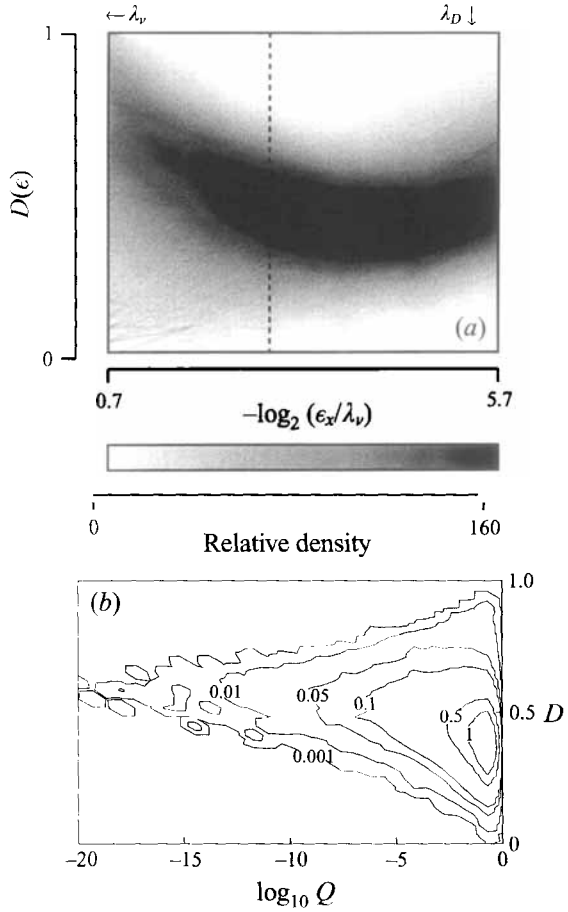

FIGURE 9. Spatial scale-similarity results for the scalar isosurface geometry at the inner scales $\lambda_D \leqslant \epsilon_x \leqslant \lambda_\nu$, showing $D(\epsilon)$ signature (*a*) and joint Q and $\langle D(\epsilon)\rangle$ signature (*b*). Compare with figures 14 and 21. Data are from over 2 million 256-point spatial intersections through conserved scalar fields $\zeta(\boldsymbol{x}, t)$ in three-dimensional (256^3) data volumes of the type in figure 1(*a*). Note the lack of any strict asymptotic approach to constant $D(\epsilon)$ with decreasing length scales ϵ_x.

in this case only 83.0% of these intersections produced values that were to the right of the contour bounding 99% of fBm sets, and slightly more than 14% of the intersections produced values that were between these contours and thus judged as being indeterminate.

It can be concluded that 256-point spatial intersections through scalar isosurface geometries in turbulent flows at length scales ϵ between the viscous and scalar diffusion scales display scale similarity that is not nearly as fractal as a Cantor set with the same record length. While there is evidence that the scaling is at least approximately similar to the stochastic fBm set, the $D(\epsilon)$ map in figure 9(*a*) gives a clear indication that the scalar isosurface geometry over this range of scales is not truly as fractal as an fBm set with the same record length, nor is its scaling as fractal as that of the dissipation support geometry over the same range of length scales.

(*a*) $\frac{\zeta_{iso}}{\langle\zeta\rangle}$	$\langle D\rangle$	σ	Fractal (%)	Random (%)	No. intersections
0.2	0.479	0.141	80.0	4.3	1 016 943
0.5	0.455	0.128	80.9	3.3	1 841 910
1.0	0.460	0.122	83.0	2.7	1 835 894
1.5	0.462	0.124	80.5	3.6	1 551 644
2.0	0.461	0.131	75.8	5.5	1 078 250
3.0	0.466	0.135	72.4	7.4	399 745
4.0	0.471	0.140	64.5	12.4	92 445

(*b*) $\frac{\chi_{sup}}{\langle\chi\rangle}$	$\langle D\rangle$	σ	Fractal (%)	Random (%)	No. intersections
0.2	0.782	0.103	98.9	0.1	2 032 930
0.5	0.691	0.124	95.0	0.4	1 996 997
1.0	0.619	0.137	89.6	1.3	1 892 537
1.5	0.576	0.143	85.7	2.3	1 773 126
2.0	0.547	0.147	82.8	2.9	1 648 085
3.0	0.508	0.152	78.1	4.1	1 410 624
4.0	0.482	0.155	74.6	4.9	1 215 872

TABLE 4. Effect of threshold values on $D(\epsilon)$ statistics and joint Q and $\langle D(\epsilon)\rangle$ statistics from intersections through (*a*) scalar isosurface geometry and (*b*) dissipation support geometry, $\chi \equiv \nabla\zeta\cdot\nabla\zeta$.

7. Effects of threshold

Scalar isosurface fields or dissipation support fields require defining a threshold scalar value ζ or scalar dissipation rate value $\nabla\zeta\cdot\nabla\zeta$. Results in the previous section were obtained by thresholding both fields at their respective mean values. This choice appears the most natural and, more importantly, in the scalar field produces near the greatest number of isoscalar crossings. The isosurface results above are thus based on the largest possible statistical sample available from the data. Nevertheless, since some previous studies have reported finding variations in dimension, and even variations in the applicability of fractal scale-similarity, based on the choice of threshold values, table 4 summarizes results from spatial analyses using various threshold levels in both the conserved scalar and scalar dissipation fields. The threshold values examined span a factor of 20 around the mean.

Results obtained for the scalar isosurface fields are given in table 4(*a*). These show that the average local fractal dimension $\langle D(\epsilon)\rangle$ and the standard deviation in local fractal dimensions σ are essentially independent of the choice of threshold level. However the percentage of intersections found to be fractal decreases significantly for threshold levels above about twice the mean scalar value. This effect appears to be due to the resulting sparseness of the isoscalar fields at higher threshold values, as can be seen from the last column of table 4 giving the number of non-empty intersections obtained for each threshold level. Note that there are nearly 20 times as many non-empty intersections for the isoscalar surface constructed from the mean scalar value as there are at four times the mean scalar value. Nevertheless, even at the highest threshold value examined, a significant fraction of the intersections satisfied the criterion for being judged to be as fractal as an fBm set of the same record length with the same average dimension, and only a small fraction of the intersections were as random as a random set with the same record length and relative cover. This demonstrates that the conclusions reached in the previous section about the scaling

properties of the isoscalar surface geometry are not specific to any narrow choice of threshold levels.

Similarly, results obtained for the scalar dissipation support geometry are given in table 4(*b*). Unlike the scalar isosurface field, in this case the largest number of non-empty intersections occurs at the lowest threshold level, for which 98.9% of intersections through the dissipation support are as fractal as 99% of fBm sets having the same record length. The decrease in average local dimension $\langle D(\epsilon)\rangle$ with increasing threshold values is to be expected from the approximately log-normal distribution of dissipation values on the support, since the support thus becomes increasingly less space-filling as the threshold increases. The standard deviation σ in average local dimension for these intersections is seen to increase slightly as the number of non-empty intersections decreases with increasing threshold value. Since this scales at least roughly as $\sigma \sim N^{-1/2}$, the effect appears to be largely a matter of statistical convergence. The fraction of non-empty intersections judged to be as fractal as a corresponding fBm set decreases significantly with increasing threshold value, and the number of intersections appearing as random as a corresponding random set increases but remains small. This may be due to the increasing sparseness of the support geometry with increasing threshold level, which reduces the amount of scaling information contained in any 256-point intersection and thus makes identification of any scale-similarity increasingly difficult. In any case, over the entire range of thresholds examined, most of the intersections are found to be as fractal as a corresponding fBm set, indicating that the fractal scaling found in the dissipation support geometry in the previous section is also not specific to any narrow choice of threshold levels.

8. Results for 256-point temporal intersections

Over 40000 individual 256-point intersections along the temporal direction through the four-dimensional data for the scalar field $\zeta(\boldsymbol{x}, t)$ and the scalar energy dissipation rate field $\nabla\zeta\cdot\nabla\zeta(\boldsymbol{x}, t)$ were analysed in an analogous manner to the spatial intersections above. The results for temporal intersections with scalar fields were generated in two ways to facilitate comparisons with previous work and with the current spatial results. Miller & Dimotakis (1991) used one-dimensional single-point time-series measurements of the scalar field to examine the set of points at which selected threshold level crossings occurred. They used one-dimensional interpolation between points in their time-series data to estimate the time at which each level crossing occurred. In the results below, their single-point construction is termed the 'isoscalar level crossing set'. Unlike their one-dimensional time series data, the present four-dimensional data allow simultaneous construction in all three space dimensions as well as in time of the true temporally evolving scalar isosurface field. In the results below, this multi-point construction is appropriately termed the 'scalar isosurface crossing set' to distinguish it from the simple isoscalar level crossing set, and to emphasize that it is the true temporal equivalent of the spatial isosurface intersections examined above.

8.1. *Scalar dissipation support*

While there are distinct differences in the isoscalar level crossing set and the scalar isosurface crossing set as defined above, there is no ambiguity whatsoever in defining the temporal support set for the true scalar dissipation field $\nabla\zeta\cdot\nabla\zeta(\boldsymbol{x}, t)$. It cannot be obtained from one-dimensional single-point time-series data, and can only be obtained from four-dimensional spatio–temporal measurements as those points where the true dissipation lies above a selected threshold value. For the results below, this threshold

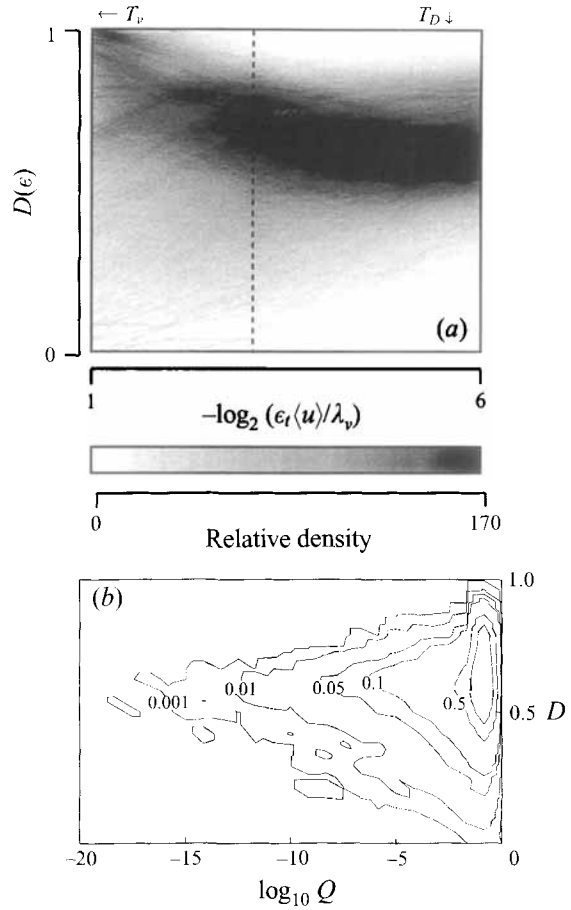

FIGURE 10. Temporal scale-similarity results for the dissipation support geometry over the inner scales $T_D \leqslant \epsilon_t \leqslant T_\nu$, showing $D(\epsilon)$ signature (*a*) and joint Q and $\langle D(\epsilon)\rangle$ signature (*b*). Compare with figures 8 and 18. Data are from over 30000 256-point temporal intersections through scalar energy dissipation fields $\nabla\zeta\cdot\nabla\zeta(x,t)$ in four-dimensional spatio–temporal data of the type in figures 2(*b*) and 2(*d*). Note the asymptotic approach to constant $D(\epsilon)$ with decreasing time scales ϵ_t.

was set at the mean dissipation value. The resulting temporal scaling properties of the dissipation support-set geometry are presented in figure 10.

Figure 10(*a*) gives the ensemble $D(\epsilon)$ results from the 256-point (temporal) dissipation support-set scaling. This can be compared with the corresponding $D(\epsilon)$ results from the 256-point (spatial) dissipation support set scaling in figure 8(*a*). The scaled length and time axes in both maps span essentially the same range of scales relative to the inner (diffusive) scale of the turbulent scalar field. This is a direct result of the essentially comparable spatial and temporal resolution in the original scalar field measurements (see §2). Figure 10(*b*) gives the ensemble joint distribution of $\langle D\rangle$ and Q values for the (temporal) dissipation support geometry, and can be compared with the corresponding result obtained from the (spatial) dissipation support geometry in figure 8(*b*). Note that the two local dimension maps in figures 8(*a*) and 10(*a*) are very similar, as are the two joint $\langle D\rangle$ and Q distributions in figures 8(*b*) and 10(*b*). The average dimension obtained in Region 2 in figure 10(*a*) is $\langle D\rangle = 0.618$, which can be compared with the value $\langle D\rangle = 0.619$ in figure 8(*a*). Similarly, the standard deviation of $D(\epsilon)$ in Region 2 in figure 10(*a*) is $\sigma = 0.139$, and in figure 8(*b*) was 0.137. Note also

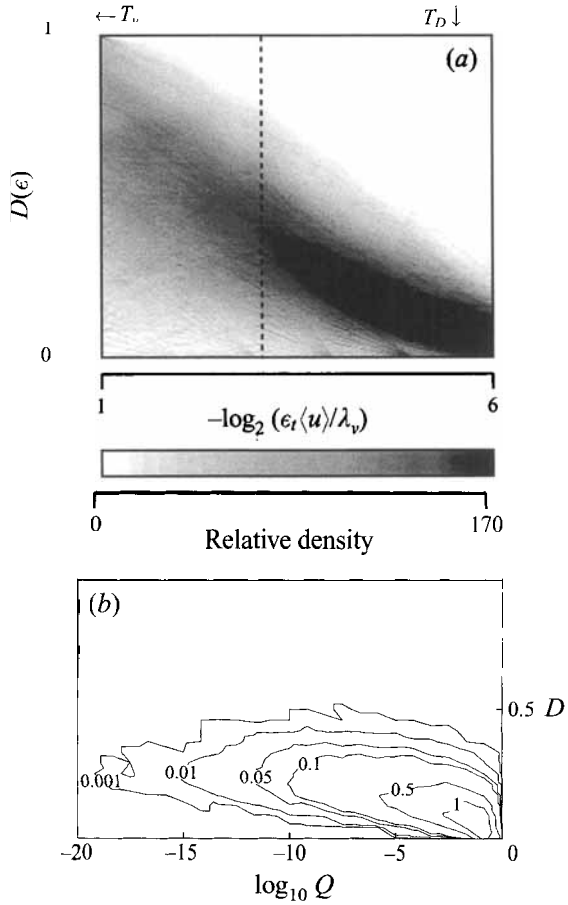

FIGURE 11. Results for isoscalar level crossings over the inner scales $T_D \leqslant \epsilon_t \leqslant T_\nu$, showing $D(\epsilon)$ signature (*a*) and joint Q and $\langle D(\epsilon)\rangle$ signature (*b*). Compare with figures 9 and 19. Data are from over 40000 256-point temporal intersections through conserved scalar fields $\zeta(\boldsymbol{x}, t)$ in four-dimensional spatio–temporal data of the type in figures 2(*a*) and 2(*c*). Note the lack of any approach to constant $D(\epsilon)$ with decreasing time scales ϵ_t, which is reflected in the Q and $\langle D(\epsilon)\rangle$ statistics as well.

that $D(\epsilon)$ clearly asymptotes to a constant value indicative of true fractal scaling. Comparing the probability contours in figure 10(*b*) with those for fBm sets and random sets in figure 6(*b*) shows that 90.8% of the $\langle D\rangle$ and Q values in figure 10(*b*) are to the right of the contour bounding 99% of the fBm sets in figure 6(*b*) (versus 89.6% for the analogous spatial intersections in figure 8*b*), and only 0.8% are to the left of the contour bounding 99% of the random sets, with less than 8.4% of the intersections producing $\langle D\rangle$ and Q values that were between these two contours. These probabilities are entirely consistent with those obtained from the (spatial) scalar dissipation support analyses above. Note that table 3 indicates a true average dimension (at infinite record length) of $D = 0.657$ for sets with scale similarity comparable to fBm sets having average dimension of 0.618 over 256-point intersections.

It can be concluded that 256-point temporal intersections through the support geometry of the scalar energy dissipation field at the inner scales of turbulent flows are nearly as fractal as scale-similar fBm sets having the same record length. Moreover, the apparent similarity of figures 8 and 10 implies the existence of a single scale similarity

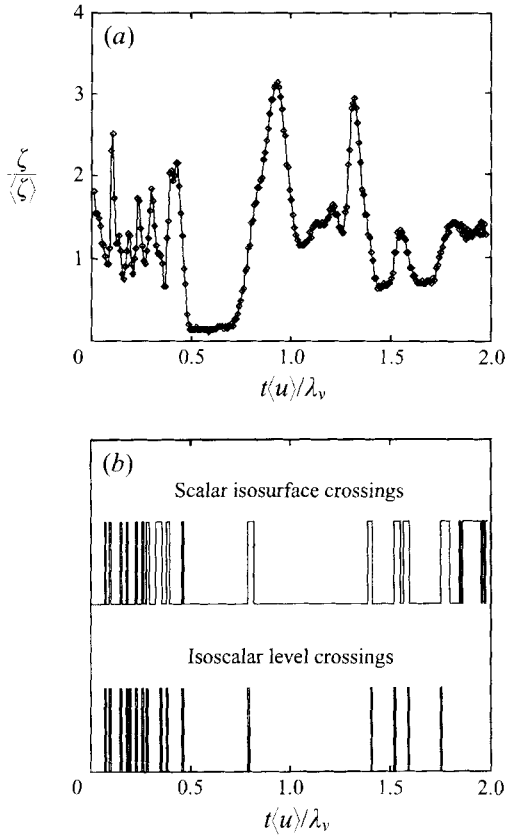

FIGURE 12. Example illustrating the difference between isoscalar level crossing sets and true scalar isosurface crossing sets. Shown are the time variation in conserved scalar values $\zeta(\boldsymbol{x}, t)$ at a single spatial location $\boldsymbol{x}$ in four-dimensional spatio–temporal data (*a*), and the corresponding isoscalar level crossing set and true scalar isosurface crossing set (*b*).

at the inner scales of turbulent flows that applies equally to both spatial and temporal aspects of the support-set geometry on which the true scalar energy dissipation rate field $\nabla\zeta\cdot\nabla\zeta(\boldsymbol{x}, t)$ is concentrated.

8.2. *Isoscalar level crossings*

Results from scale similarity analyses of 256-point temporal isoscalar level crossing sets, as defined above, are given in figure 11. These results can be compared with the local dimension map for an fBm set in figure 5(*b*) and the joint $\langle D\rangle$ and Q distribution for fBm sets in figure 6(*b*). It is readily apparent that the local dimension $D(\epsilon)$ in figure 11(*a*) is fundamentally different from any of the maps for known fractal sets or from the experimental data above. The ensemble $D(\epsilon)$ results show no asymptote to any constant dimension as would be seen if fractal scale-similarity applied to this construct, and instead decrease monotonically to $D\rightarrow 0$ as $\epsilon\rightarrow 0$. Similarly, the joint distribution of $\langle D\rangle$ and Q values falls in the range where both random and fBm sets coincide, leaving the clear conclusion that these isoscalar level crossing sets are not fractal.

These results for level crossing sets are in complete agreement with those of Miller & Dimotakis (1991), who based their assessment of fractal scale-similarity in turbulent

flows entirely on isoscalar level crossing sets. In particular, the local dimension map $D(\epsilon)$ in figure 11(*a*) can be compared with their figures 5, 8 and 17, and shows the same lack of any constant region that would be indicative of fractal scaling. However, while they suggested that this was indicative of a broad inapplicability of fractal scale-similarity in turbulent flows, the present results demonstrate that this lack of fractal scale-similarity is particular to the isoscalar level crossing construct, and is not indicative of a lack of fractal scale-similarity in turbulent flows in general. Indeed, scale-similarity tests applied to other constructs, like the true scalar isosurface geometry and in particular the scalar dissipation support geometry, obtained from precisely the same data as the isoscalar level crossing sets, clearly show much closer agreement with stochastic fractal similarity in both spatial and temporal intersections at the inner scales of turbulent flows. These can be compared with the corresponding scaling results for one-dimensional spatial isoscalar level crossings in figure 6 of Miller & Dimotakis (1991) and for mixed spatial and temporal isoscalar level crossings in their figure 7. Lacking the three-dimensional spatial information necessary to identify true isoscalar surfaces with discrete data, their constructs show the same clearly non-fractal scaling as do our level crossing results in figure 11.

8.3. *Scalar isosurface crossings*

In this subsection, analogous results are presented for 256-point temporal scalar isosurface crossing sets, from the present four-dimensional scalar field measurements. As noted above, this set is different from the various isoscalar level crossing sets considered by Miller & Dimotakis (1991). This is illustrated in figure 12: a short sample of the temporal scalar field data are shown in figure 12(*a*), together with the corresponding isoscalar level crossing set and the corresponding scalar isosurface crossing set in figure 12(*b*). Note that the availability of additional three-dimensional spatial information from surrounding pixels in the scalar isosurface construction allows the true isosurface to be determined, and thus a more precise determination of the length of time it takes the isosurface to cross the pixel of interest. Isoscalar level crossing sets from one-dimensional single-point time-series data, on the other hand, are constructed without this additional spatial information and thus are a more coarse approximation of the precise time during which the chosen isoscalar value resides in the pixel volume. Isoscalar level crossing sets constructed solely from one-dimensional spatial measurements suffer the analogous spatial problem. In the dual limits of infinite digital resolution and infinite spatio-temporal resolution, the two constructions become identical. However for any finite-resolution discrete measurement (including any fully resolved measurement) there is an uncertainty of up to one pixel width in locating both the isosurface and the true threshold crossing point. With one-dimensional temporal or spatial data, any greater precision than this requires *ad hoc* approximation. However, with three-dimensional spatial data it is possible to determine if the isosurface still occupies the pixel volume. This distinction creates important differences in these two sets, which in turn lead to substantial differences in their respective scale similarity properties.

The latter point is illustrated in figure 13, where the covering properties $N(\epsilon)$ of the two sets in figure 12(*b*) are compared in figure 13(*a*) and their corresponding local dimensions are compared in figure 13(*b*). Note that there are large differences between the results for these two sets. In particular, the local dimension $D(\epsilon)$ in figure 13(*b*) shows a monotonic decrease to $D \to 0$ as $\epsilon \to 0$ for the isoscalar level crossing set, as was seen in figure 11(*a*) for an ensemble of such isoscalar levels crossing sets, but shows a more nearly constant region of $D(\epsilon)$ for the scalar isosurface crossing set. The

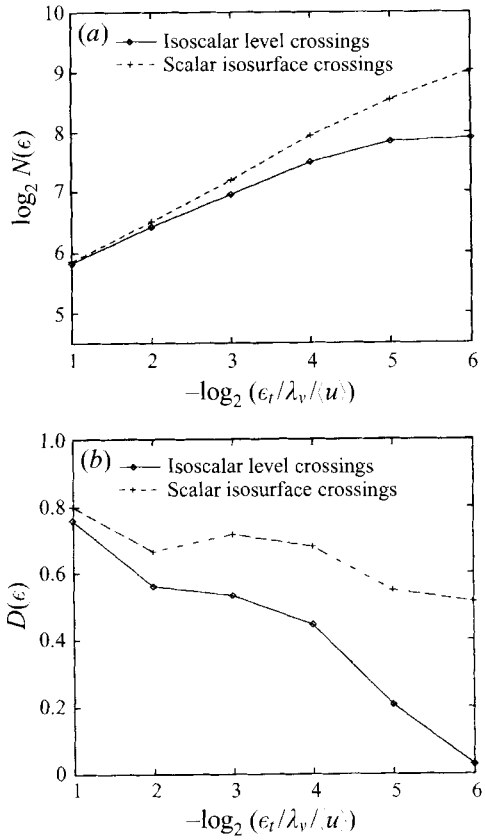

FIGURE 13. Results from analyses of the isoscalar level crossing set and true scalar isosurface crossing set in figure 12, showing the corresponding $\log_2 N(\epsilon)$ signatures (*a*) and $D(\epsilon)$ signatures (*b*). At sufficiently large scales the two sets become identical, as evidenced above, but at small scales the two show fundamentally different scalings.

difference between these two constructs, and in particular their differing scale-similarity properties, appears to explain why the earlier study by Miller & Dimotakis (1991) concluded that fractal scaling was inapplicable to turbulent flows, while figure 9(*b*) clearly shows at least limited stochastic fractal scale-similarity for the true scalar isosurface geometry at the inner scales of turbulent flows.

Figure 14(*a*) gives the ensemble $D(\epsilon)$ results from 256-point (temporal) scalar isosurface crossing sets, and can be compared with the corresponding $D(\epsilon)$ results from the 256-point (spatial) isoscalar surface geometry scaling in figure 9(*a*). The scaled length and time axes in both maps again span essentially the same range of scales relative to the inner (diffusive) scale of the turbulent scalar field. Figure 14(*b*) gives the ensemble joint distribution of $\langle D \rangle$ and Q values for the (temporal) scalar isosurface crossing sets, and can be compared with the corresponding result obtained from the (spatial) isoscalar surface geometry scaling in figure 9(*b*). As was the case in comparisons of the spatial and temporal scale similarity in the scalar dissipation support sets in figures 8 and 10, note that the results in figures 9(*a*) and 14(*a*) are very similar, as are the two joint $\langle D \rangle$ and Q distributions in figures 9(*b*) and 14(*b*). The average dimension $\langle D \rangle$ in Region 2 in figure 14(*a*) is 0.453, which can be compared with the value 0.460 in figure 9(*a*). Similarly, the standard deviation σ in Region 2 in figure 14(*a*) is 0.129, and in figure 9(*b*) was 0.122. Comparing probability contours in

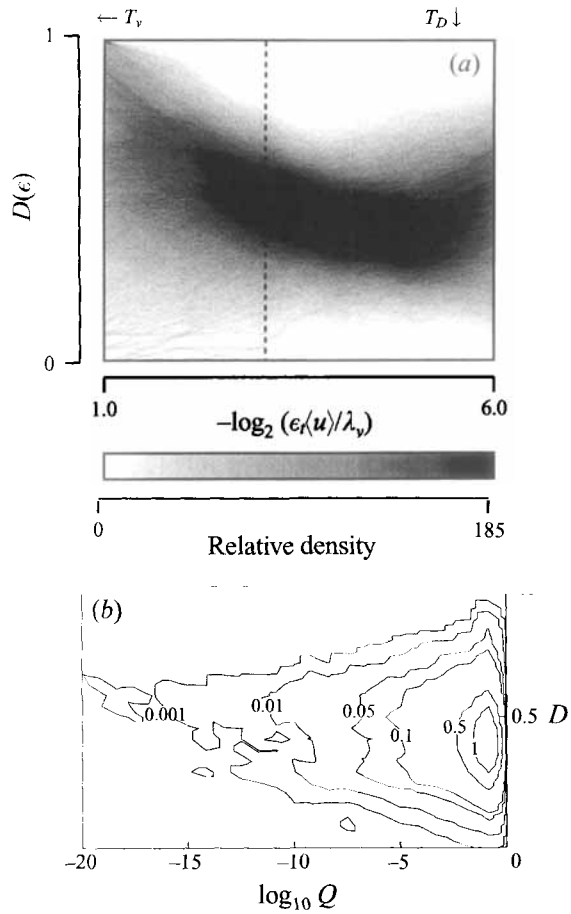

FIGURE 14. Temporal-scale similarity results for the true scalar isosurface geometry over the inner scales $T_D \leqslant \epsilon_r \leqslant T_\nu$, showing $D(\epsilon)$ signature (*a*) and joint Q and $\langle D(\epsilon)\rangle$ signature (*b*). Compare with figures 9, 11 and 21. Data are from over 40000 256-point temporal intersections through conserved scalar fields $\zeta(x, t)$ in four-dimensional spatio–temporal data. Note the lack of any strict asymptotic approach to constant $D(\epsilon)$ with decreasing length scales ϵ_r.

figure 14(*b*) with the results for fBm sets and random sets in figure 6(*b*) shows that 85.7% of the $\langle D\rangle$ and Q values from the (temporal) scalar isosurface crossing sets are to the right of the contour bounding 99% of the fBm sets, and only 1.8% are to the left of the contour bounding 99% of the random sets. These probabilities are very close to those obtained from the (spatial) scalar isosurface geometry analyses above.

It can be concluded that 256-point temporal scalar isosurface crossing sets at the inner scales of turbulent flows agree very well with the corresponding 256-point spatial intersections through the isoscalar surface geometry. As was found by comparing results from spatial and temporal analyses of scalar dissipation support-set geometries at the inner scales of turbulent flows, this observation further implies the existence of a single scale-similarity at the inner scales of turbulent flows that applies equally to both spatial and temporal aspects of the isoscalar surface geometry. However the $D(\epsilon)$ map in figure 14(*a*) again shows that there is no clear asymptote to a constant dimension that would be indicative of true fractal scaling. Thus, as was found from the spatial analyses in §6, the notion of stochastic scale similarity of the fBm type is at best an approximation for the isoscalar surface geometry over the inner range of

spatio–temporal scales. This is in contrast to the results in figure 10(*a*) for the scalar dissipation support geometry, where analyses of 256-point records showed a more convincing asymptote to constant $D(\epsilon)$ indicative of genuine stochastic fractal scale-similarity.

9. Results for 4096-point temporal intersections

The results above have dealt with assessments of spatial scale similarity among the range of length scales between λ_ν and λ_D, and temporal scale similarity among the range of time scales between T_ν and T_D, which comprise the inner scales of turbulent scalar fields. The analyses have made use of 256-point spatial and temporal data records which span precisely this range of scales. In this section, these scale similarity analyses are extended to much larger scales by using longer 4096-point temporal records that span the range of temporal scales from the local large-scale time T_δ to the scalar diffusive scale T_D. Results in each case are from nearly 2000 such 4096-point temporal intersections.

The longer data records of course lead to reduced variance in the local fractal dimension $D(\epsilon)$, and thus require recalibrating the local fractal dimension maps using 4096-point fBm level crossing sets. An example of the resulting $D(\epsilon)$ maps, from 10000 realizations of fBm sets with $D = 0.5$, is shown in figure 15. This can be compared with the 256-point results for Cantor and fBm sets with $D = 0.5$ in figures 4(*b*) and 5(*b*).

9.1. *Scalar dissipation support*

Figure 16(*a*) gives the ensemble $D(\epsilon)$ results from 4096-point temporal intersections through the scalar dissipation support over the range of scales from T_δ to T_D. This should be compared with the signature for fBm sets with a single fixed dimension in figure 15, and that from the shorter-record-length spatial and temporal results in figures 8(*a*) and 10(*a*). The result in figure 16(*a*) might appear to suggest a different scale-similarity among scales between T_δ and T_ν and among the inner scales between T_ν and τ_D, somewhat reminiscent of the differing self-similarities in these two scale regimes that lead to the $k^{-5/3}$ and k^{-1} spectral scalings, respectively, alluded to in the Introduction. However, to clarify this figure 17(*a*) shows the $D(\epsilon)$ signature for 10000 4096-point fBm sets all having the same dimension $D = 0.618$ as the average value from the temporal dissipation support results above. Note that even in this manifestly fractal case, the $D(\epsilon)$ results at this dimension and with this longer record length show only a slow asymptotic approach to the constant dimension indicative of fractal scaling. It must be concluded that the decreasing $D(\epsilon)$ values obtained over the same range of scales in figure 16(*a*) are not necessarily indicative of non-fractal scaling at temporal scales between T_δ and T_ν.

This is further supported by figure 16(*b*), which gives the corresponding joint distribution of $\langle D \rangle$ and Q values for the dissipation support set over $T_D \leqslant \epsilon_t \leqslant T_\delta$, where the reduced variation in local dimension noted above is evident, and where the longer record lengths lead to much higher Q values as well. The result is a much narrower joint distribution. In fact the distribution very nearly resembles the result in figure 17(*b*) for 4096-point fBm sets with a single dimension. Figure 17(*c*) shows the corresponding probability contours over a wide range of dimensions, where 99.0% of the long-record-length intersections in figure 16 yield $\langle D \rangle$ and Q values to the right of the contour bounding 99% of the fBm sets in figure 17(*c*). No intersections produced values to the left of the contour bounding 99% of all corresponding random sets. Thus essentially all of the scalar dissipation support set, even at temporal scales between T_δ

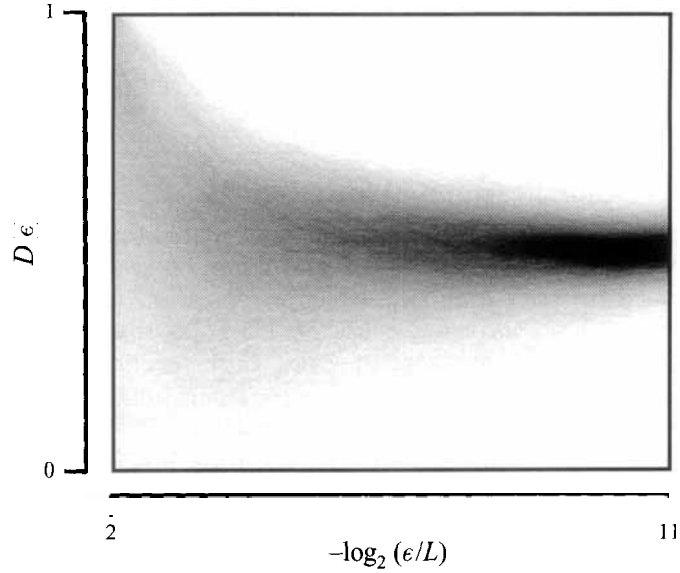

FIGURE 15. $D(\epsilon)$ signature for stochastically self-similar fBm sets with $D = 0.5$ and 4096-point record lengths. Compare with the corresponding results for 256-point record lengths in figure 5.

and T_ν, produces 4096-point intersections that are as fractal as an fBm set having the same record length.

The range of scales between T_ν and T_D is shown in figure 18, where the present result can be seen to be in good agreement with the 256-point spatial result in figure 8(*a*) and the corresponding temporal result in figure 10(*a*), but with the longer record length giving less variance in local dimension. The average dimension $\langle D(\epsilon)\rangle$ in Region 2 from the 4096-point intersections is 0.661, with the variance giving $\sigma = 0.047$, which can be compared with the 0.619 ± 0.138 result from the 256-point intersections. The higher dimension from the longer record lengths is to be expected from table 3, in which $\langle D(\epsilon)\rangle = 0.619$ from 256-point records would indicate a true dimension at infinite record length of $D = 0.658$, in excellent agreement with the present 4096-point result. It must be concluded that the geometry of the scalar dissipation support on the inner scales of turbulent flows has very nearly the same scale-similarity properties as does the stochastically self-similar fBm fractal set with $D = 0.66$. The similarities demonstrated above between spatial and temporal scaling properties of the scalar dissipation support indicates that this conclusion applies to the entire four-dimensional spatio–temporal geometry of the support set on which the scalar dissipation field in turbulent flows is concentrated. Moreover, this dimension value appears consistent with findings of Prasad, Meneveau & Sreenivasan (1988) from multifractal analysis of their approximated scalar dissipation rate, where a dimension estimate of 0.70 results for the set that dominates the mean dissipation (see their figure 5 for $q = 1$).

9.2. *Isoscalar level crossings*

Figure 19(*a*) presents the ensemble $D(\epsilon)$ results over the range of scales from T_δ to T_D, obtained from 4096-point temporal isoscalar level crossing sets of the type analysed by Miller & Dimotakis (1991) and in §8.2. The corresponding joint distribution of $\langle D\rangle$ and Q values is shown in figure 19(*b*). It is readily apparent that both these results are inconsistent with any notion of fractal scale-similarity in isoscalar level crossing sets in turbulent flows, even over the inner range of scales from T_ν to T_D. This is in complete

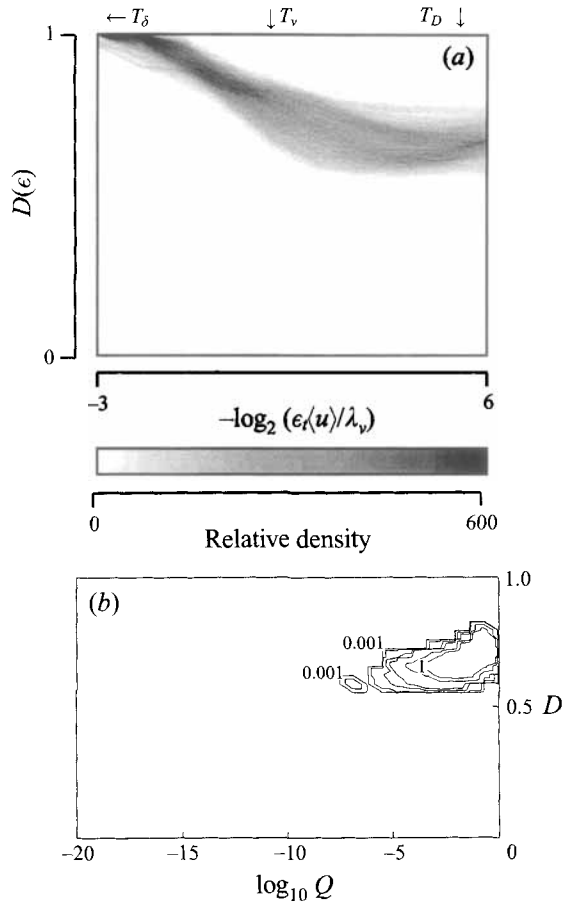

FIGURE 16. Temporal scale-similarity results for the dissipation support geometry over the range of scales from $T_D \leqslant \epsilon_r \leqslant T_\delta$, showing $D(\epsilon)$ signature (*a*) and joint Q and $\langle D(\epsilon)\rangle$ signature (*b*). Compare with figures 10 and 17. Data are from 4096-point temporal intersections through scalar energy dissipation fields $\nabla\zeta\cdot\nabla\zeta(x,t)$ in four-dimensional spatio–temporal data of the type in figures 2(*b*) and 2(*d*).

agreement with the result of Miller & Dimotakis for the same construct, and in fact the present figure 19(*a*) is essentially identical to their figure 5. This result is also in agreement with the corresponding result from 256-point record lengths in figure 11(*a*), with the reduced variance from the present longer record lengths more clearly revealing the monotonic decrease to $D \to 0$ as $\epsilon \to 0$. However while Miller & Dimotakis suggest that this lack of fractal scale-similarity in temporal isoscalar level crossing sets broadly precludes fractal scale-similarity in turbulent flows, the present results verify that this is not the case. The results above for intersections through the scalar dissipation support, obtained from precisely the same data, clearly show scale-similarity that is as fractal as an fBm set having the same record length.

9.3. *Scalar isosurface crossings*

Figure 20(*a*) presents the ensemble $D(\epsilon)$ results from 4096-point temporal intersections through the true scalar isosurface geometry over the range of scales from T_δ to T_D. Note that, between T_δ and T_ν, the results for scalar isosurface geometry, figure 20(*a*) are essentially identical to those for the isoscalar level crossings in figure 19(*a*). This is to

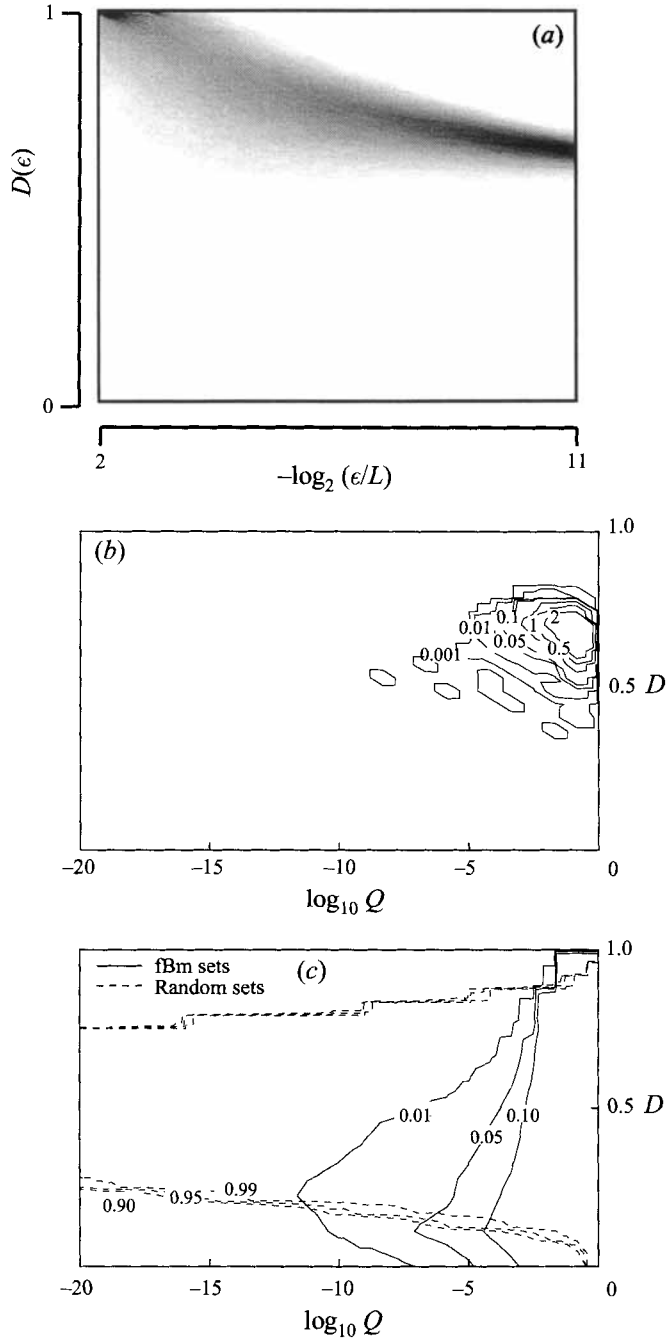

FIGURE 17. Box counting results for stochastically self-similar fBm sets with 4096-point record lengths, showing $D(\epsilon)$ signature for $D \equiv 0.618$ (*a*), joint Q and $\langle D(\epsilon) \rangle$ signature for $D \equiv 0.618$ (*b*), and joint Q and $\langle D(\epsilon) \rangle$ signature for wide range of dimensions (*c*). Compare with figures 16 and 18–21. Note the asymptotic approach to constant $D(\epsilon)$ with decreasing scale ϵ.

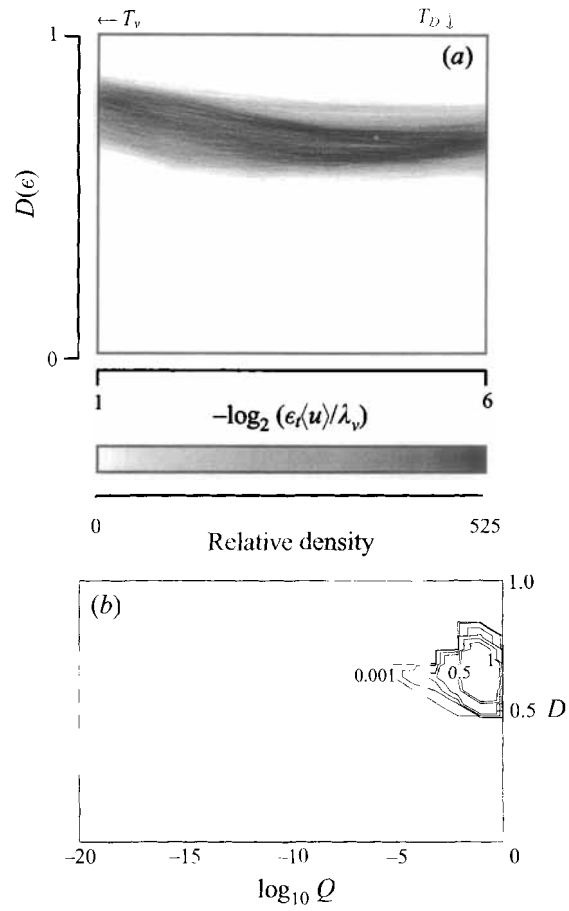

FIGURE 18. Results from figure 16 over the inner range of scales $T_D \leqslant \epsilon_\tau \leqslant T_\nu$, showing $D(\epsilon)$ signature (a) and joint Q and $\langle D(\epsilon)\rangle$ signature (b). Compare with figure 17. Data are from 4096-point temporal intersections through scalar energy dissipation fields $\nabla\zeta\cdot\nabla\zeta(\boldsymbol{x}, t)$.

be expected, since the differences between these two constructs are at the small scales. Indeed, over the range of inner scales from T_ν to T_D there are fundamental differences between the $D(\epsilon)$ results in figures 19(a) and 20(a), consistent with the examples in figures 12 and 13 and the results in figures 11 and 14.

The $D(\epsilon)$ results over the inner range of scales from T_ν to T_D are shown in figure 21. Comparing with the corresponding 256-point results in figures 9(a) and 14(a) shows good agreement at the inner scales, with the longer record length giving less variance in local dimension. This reduced variance makes clearer the lack of a strict approach to a truly constant dimension indicative of genuine fractal scale-similarity over this range of scales.

At larger scales, between T_δ and T_ν, the $D(\epsilon)$ result in figure 20(a) may not look very different from that in figure 16(a); however examining contours in the joint distribution of $\langle D\rangle$ and Q values in figure 20(b) and comparing with figures 16 and 17(b) shows that it is difficult to find a 4096-point scalar isosurface intersection extending over T_δ to T_D that is as fractal as a corresponding fBm set over this range of scales. Only 2.6% of the intersections produced $\langle D\rangle$ and Q values to the right of the contour bounding 99% of all fBm sets having the same record length. It must be concluded that scalar isosurface fields in turbulent flows display scaling that at least approximates stochastic

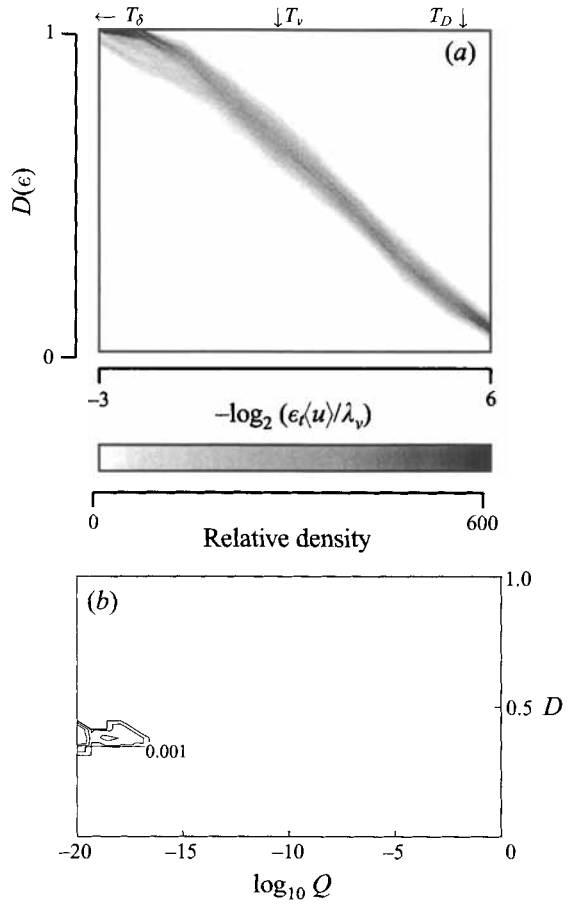

FIGURE 19. Results from analyses of isoscalar level crossings over the range of scales from $T_D \leqslant \epsilon_\tau \leqslant T_\delta$, showing $D(\epsilon)$ signature (*a*) and joint Q and $\langle D(\epsilon)\rangle$ signature (*b*). Compare with figures 11, 17 and 20. Data are from 4096-point temporal intersections through conserved scalar fields $\zeta(\boldsymbol{x}, t)$ in four-dimensional spatio–temporal data of the type in figures 2(*a*) and 2(*c*). Note the lack of any approach to constant $D(\epsilon)$ with decreasing time scales ϵ_t, which is reflected in the joint Q and $\langle D(\epsilon)\rangle$ statistics as well.

fBm fractal scale-similarity only over spatio–temporal regions of the order of the inner length and time scales (λ_D, T_D) to (λ_ν, T_ν), but do not display a single fractal scaling for records spanning across much larger spatio–temporal regions.

10. Discussion and conclusions

This paper has developed objective statistical techniques for scale-similarity analyses and applied them to 256-point and 4096-point data records. The goal has been to assess the applicability of uniform fractal scale-similarity in the spatio–temporal structure of $Sc \gg 1$ conserved scalar and scalar dissipation fields in turbulent flows. The techniques developed here have been shown to reliably identify both deterministic (Cantor) and stochastic (fBm) fractal sets, and robustly discriminate between fractal and random sets even for short record lengths. These techniques have been applied to one-dimensional spatial and temporal intersections from fully resolved three- and four-dimensional measurements of conserved scalar fields $\zeta(\boldsymbol{x}, t)$ and scalar energy

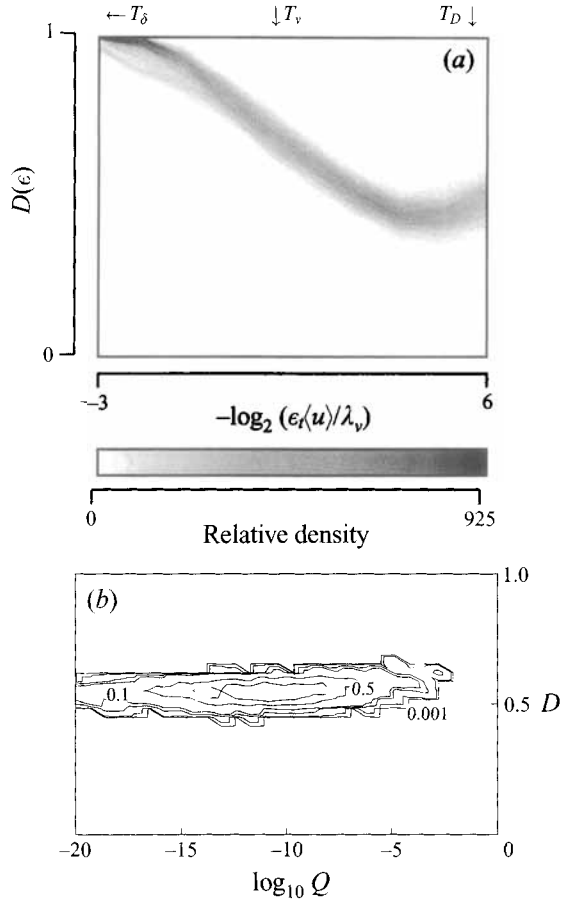

FIGURE 20. Temporal scale-similarity results for the true scalar isosurface geometry over the range of scales from $T_D \leqslant \epsilon_t \leqslant T_\delta$, showing $D(\epsilon)$ signature (*a*) and joint Q and $\langle D(\epsilon)\rangle$ signature (*b*). Compare with figures 14, 16 and 17. Data are from 4096-point temporal intersections through conserved scalar fields $\zeta(\boldsymbol{x}, t)$ in four-dimensional spatio–temporal data. Note the lack of any asymptotic approach to constant $D(\epsilon)$ with decreasing length scales ϵ_t, even over the inner scales $T_D \leqslant \epsilon_t \leqslant T_\nu$.

dissipation rate fields $\nabla\zeta\cdot\nabla\zeta(\boldsymbol{x}, t)$ in a turbulent flow. The results obtained span the range of scales from the scalar diffusion scales (λ_D, T_D) to the viscous diffusion scales (λ_ν, T_ν) and to the outer scales (δ, T_δ), and are summarized in table 5.

From the spatio–temporal support geometry on which the scalar dissipation field $\nabla\zeta\cdot\nabla\zeta(\boldsymbol{x}, t)$ is concentrated at the inner range of scales between (λ_D, T_D) and (λ_ν, T_ν), 89.6% of more than 2 million spatial intersections and 90.8% of more than 20000 temporal intersections were found to display uniform scale-similarity as fractal as stochastically self-similar fBm sets having the same record length. However, these intersections were not as fractal as deterministically self-similar irregular Cantor sets having the same record length. Nevertheless, only 1.3% of such spatial intersections and 0.8% of temporal intersections showed scale-similarity characteristics as random as a corresponding random set. Both the 256-point spatial and temporal intersections in figures 8 and 10 showed the same average local fractal dimension $\langle D(\epsilon)\rangle$ and standard deviation σ, yielding 0.619 ± 0.138 in comparably normalized length and time scales in Region 2. From table 3 this would indicate a true average dimension (at infinite record length) of $D = 0.658$ for intersections with the spatio–temporal

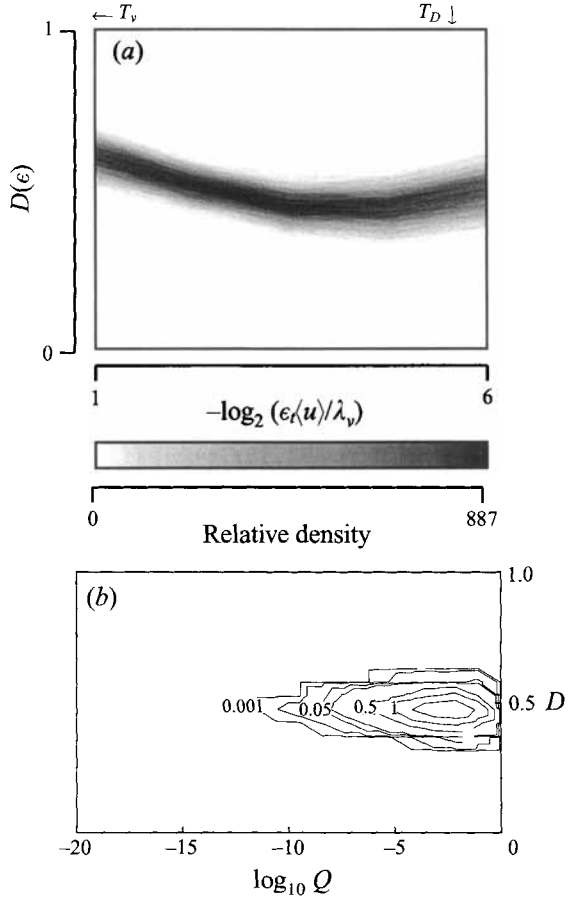

FIGURE 21. Results from figure 20 over the inner range of scales $T_D \leqslant \epsilon_t \leqslant T_\nu$, showing $D(\epsilon)$ signature (*a*) and joint Q and $\langle D(\epsilon)\rangle$ signature (*b*). Compare with figures 9, 14 and 18. Data are from 4096-point temporal intersections through conserved scalar fields $\zeta(\boldsymbol{x}, t)$ in four-dimensional spatio–temporal data. Note the lack of any strict asymptotic approach to constant $D(\epsilon)$ with decreasing length scales ϵ_t.

		$\langle D\rangle$	σ	Fractal (%)	Random (%)
256-point records	Spatial support	0.619	0.137	89.6	1.3
	Temporal support	0.618	0.139	90.8	0.8
	Spatial isosurface	0.460	0.122	83.0	2.7
	Temporal isosurface	0.453	0.129	85.7	1.8
	Temporal level crossings	—	—	13.8	15.2
4096-point records	Temporal support	0.661	0.047	99.0	0.0
	Temporal isosurface	0.466	0.039	2.6	0.0
	Temporal level crossings	—	—	0.0	0.0

TABLE 5. Summary of variations in applicability of stochastic fractal scale-similarity and dimension in Region 2 for sets analysed. Note that the average dimension $\langle D\rangle = 0.619$ from 256-point dissipation support records corresponds in table 3 to $D = 0.658$ for fBm sets with effectively infinite record length, which agrees well with $\langle D\rangle = 0.661$ from 4096-point dissipation support records.

dissipation support geometry at the inner scales of turbulent flows. This is in good agreement with the value $\langle D(\epsilon)\rangle = 0.661 \pm 0.047$ from 4096-point temporal results in Region 2 in figure 18, for which 99.0% of all intersections demonstrated scale similarity as fractal as 99% of all fBm sets with the same record length. As noted in §9.1, this value for the dissipation support dimension appears to be in good agreement with the result inferred from the approximate multifractal analyses of Prasad *et al.* (1988). The present results for the dimension at threshold values other than the mean dissipation can be inferred from table 4(*b*).

At larger scales, between the viscous and outer scales T_ν and T_δ, figure 16(*b*) shows that the scalar dissipation support geometry continues to display scale-similarity as fractal as fBm fractal sets having the same record length. The similarity found throughout this study between comparably scaled spatial and temporal intersections would indicate that this scale-similarity applies to spatial scales between λ_ν and δ as well. In fact comparing figures 16 and 17(*b*) suggests that a single dimension might even suffice to model the dissipation support geometry over the entire range of scales from (λ_D, T_D) to (δ, T_δ).

Similar analyses of the geometry of true scalar isosurfaces in the conserved scalar field $\zeta(x, t)$ over the inner range of spatio–temporal scales between (λ_D, T_D) and (λ_ν, T_ν) do not show a strict asymptotic approach to constant dimension with decreasing scale such as seen in the dissipation support geometry. However over the inner scales (see figures 9, 14, and 21) such isosurfaces display scaling in both space and time that at least approximates the similarity characteristics of an fBm set with $D = 0.48$ (at infinite record length), with table 4(*a*) showing that the corresponding dimension for other isoscalar values remains essentially the same. Of over 2 million such spatial intersections, 83.0% showed scale-similarity as fractal as 99% of fBm sets of the same record length, as did 85.7% of over 2×10^6 such temporal intersections. In both cases, less than 3% of these intersections showed scaling as random as a corresponding random set.

However unlike the scalar dissipation support geometry, at scales between the viscous scale T_ν and the outer scale T_δ, figure 20(*b*) demonstrates that the scalar isosurface geometry shows no uniform scale-similarity consistent with either deterministically self-similar fractals such as the irregular Cantor set or stochastically self-similar fractals such as the fBm set. Only 2.6% of all intersections spanning between T_ν and T_δ were as fractal as fBm sets of the same record length. In view of the consistency between spatial and temporal results found throughout this study, it must be expected that this lack of uniform fractal scale-similarity in isoscalar surface geometry applies to the corresponding range of spatial scales between λ_ν and δ as well.

The reason for this apparently fundamental difference in scale similarity properties of the conserved scalar field $\zeta(x, t)$ and the scalar dissipation rate field $\nabla\zeta \cdot \nabla\zeta(x, t)$ may lie in the differing retention of information in these two fields. In the scalar field, the precise spatial distribution of scalar values, and thus also the isosurface geometry, depends intimately on the entire evolution of the scalar field since its initial conditions. In contrast, the scalar dissipation support geometry is largely insensitive to all but its recent history, since as scalar gradient layers merge and their dissipation drops below the threshold value, they disappear from the support set and the information they carry concerning past history of the underlying mixing dynamics is lost. Scalar isosurface geometries thus reflect variations in the dimension of the underlying multiplicative process that produces the mixing, while the dissipation support field would not.

While the strong evidence of fractal-scale similarity with $D = 0.66$ in the scalar dissipation support appears consistent with the result of Prasad *et al.* (1988), the apparent lack of any uniform fractal scale-similarity in the geometry of isoscalar

surfaces contrasts with the findings of Sreenivasan & Meneveau (1986), Prasad & Sreenivasan (1990), Sreenivasan *et al.* (1989) and Sreenivasan (1991). There are several possible reasons for the different finding in this study. The present assessments are based on strict tests for uniform fractal scale-similarity over the entire range of scales examined. That no such scaling is found in the isoscalar surface geometries could potentially result from a break in similarity over the range of scales examined. Indeed a scaling break might be anticipated across the viscous diffusion scales (λ_ν, T_ν), where the scalar energy spectrum changes from k^{-1} to $k^{-5/3}$ scalings and where Sreenivasan and co-workers show evidence for a corresponding change in the fractal dimension. However the present results convincingly show uniform fractal scale-similarity in the dissipation support field over the entire range of scales examined, and show no change in dimension across (λ_ν, T_ν). A second possible reason for the different finding in this study is the potential influence of inner and outer cutoffs in the range of scales examined. The inner cutoff near the scalar diffusion scales (λ_D, T_D) lies at the extreme end of the range of scales examined, and moreover it is precisely in this inner range of scales that the present study finds the closest approach to uniform fractal scale similarity. The other cutoff expected near (δ, T_δ), lies somewhat outside the range of scales examined, even in the longer 4096-point temporal records. Moreover strong evidence was found for fractal scale-similarity in the dissipation support field over this entire range of scales (see figure 16*b*), yet over the same range of scales no evidence of fractal scale-similarity was found in the corresponding scalar isosurface data (see figure 20*b*). It is of course possible that the cutoff scales or even the break in scaling across the viscous scales manifest themselves differently in the scalar and dissipation fields, as discussed above. There also remains a possibility that the present Re_δ values may not be sufficiently large for the scale-similarity to establish itself in the scalar field; however these Reynolds numbers are not very different from other studies, and more importantly the clear evidence for uniform fractal scale-similarity in the dissipation support fields from precisely the same data suggests that this is not likely to be the case. Finally, it is possible that the strict statistical criterion adopted here for judging data records to be as fractal as various test sets having the same record lengths may be more stringent than those applied in previous studies.

The present study has also clarified some of the apparent contradictions between earlier results for the applicability of fractal scaling concepts to turbulent scalar fields. In particular the results have shown that, except in the double limit of infinite digital resolution and infinite spatial and temporal resolution, isoscalar level crossing sets are fundamentally different constructs from the true scalar isosurface sets examined herein and in the other studies cited. These two constructs differe at the small scales only, but this leads to fundamentally different scale-similarities as was shown in figures 11 and 14 and figures 19 and 20. Level crossing sets cannot be compared against true scalar isosurface intersections to judge the applicability of fractal scale-similarity in turbulent flows. The present results have clearly demonstrated that, while isoscalar level crossing sets show no fractal scale-similarity, intersections through the scalar dissipation support geometry obtained from precisely the same data show scale-similarity consistent with stochastic fractal sets having the same record length.

The three- and four-dimensional scalar field data used in this study were obtained at Michigan as part of the doctoral dissertation work of Dr Kenneth B. Southerland, under support from the Air Force Office of Scientific Research (AFOSR) Airbreathing Combustion program under Grant No. AFOSR-89-0541 and the AFOSR Turbulence Structure and Control program under Grant No. F49620-92-J-0025, and under

support from the Gas Research Institute (GRI) under GRI Contract No. 5087-260-1443.

REFERENCES

BATCHELOR, G. K. 1959 Small-scale variation of convected quantities like temperature in turbulent fluid. *J. Fluid Mech.* **5**, 113–139.

BENZI, R., PALADIN, G., PARISI, G. & VULPIANI, A. 1984 On the multifractal nature of fully developed turbulence and chaotic systems. *J. Phys.* A: *Math. Nucl. Gen.* **17**, 3521–3531.

BEVINGTON, P. R. & ROBINSON, D. K. 1992 *Data Reduction and Error Analysis in the Physical Sciences*. McGraw-Hill.

DAHM, W. J. A., SOUTHERLAND, K. B. & BUCH, K. A. 1991 Direct, high-resolution, four-dimensional measurements of the fine scale structure of $Sc \gg 1$ molecular mixing in turbulent flows. *Phys. Fluids* A **3**, 1115–1127.

DOWLING, D. R. 1991 The estimated scalar dissipation rate in gas-phase turbulent jets. *Phys. Fluids* A **3**, 2229–2246.

DUBUC, B., QUINIOU, J. F., ROQUES-CARMES, C., TRICOT, C. & ZUCKER, S. W. 1989 Evaluating the fractal dimension of profiles. *Phys. Rev.* A **39**, 1500–1512.

FEDER, J. 1988 *Fractals*. Plenum Press.

FREDERIKSEN, R. D., DAHM, W. J. A. & DOWLING, D. R. 1997*a* Experimental assessment of fractal scale similarity in turbulent flows. Part 2. Higher-dimensional intersections and non-fractal inclusions. *J. Fluid Mech.* (to appear).

FREDERIKSEN, R. D., DAHM, W. J. A. & DOWLING, D. R. 1997*b* Experimental assessment of fractal scale similarity in turbulent flows. Part 3. Multifractal scaling. *J. Fluid Mech.* (to appear).

FRISCH, U. & PARISI, G. 1985 In *Turbulence and Predictability in Geophysical Fluid Mechanics and Climate Dynamics* (ed. M. Ghil, R. Benzi & G. Parisi). North-Holland.

FRISCH, U., SULEM, P. L. & NELKIN, M. 1978 A simple dynamical model of intermittent fully developed turbulence. *J. Fluid Mech.* **87**, 719–736.

GRASSBERGER, P. 1983 Generalized dimensions of strange attractors. *Phys. Lett.* A **97**, 227–230.

HALSEY, T. C., JENSEN, M. H., KADANOFF, L. P., PROCACCIA, I. & SHRAIMAN, B. I. 1986 Fractal measures and their singularities: The characterization of strange sets. *Phys. Rev.* A **33**, 1141–1151.

HENTSCHEL, H. G. E. & PROCACCIA, I. 1983 The infinite number of generalized dimensions of fractals and strange attractors. *Physica* D **8**, 435–444.

JIMÉNEZ, J., WRAY, A. A., SAFFMAN, P. G. & ROGALLO, R. S. 1993 The structure of intense vorticity in isotropic turbulence. *J. Fluid Mech.* **255**, 65–90.

KOLMOGOROV, A. N. 1941 Local structure of turbulence in an incompressible fluid at very high Reynolds numbers. *C.R. Acad. Sci. URSS* **30**, 301–305.

LANE-SERFF, G. F. 1993 Investigation of the fractal structure of jets and plumes. *J. Fluid Mech.* **249**, 521–534.

MANDELBROT, B. B. 1974 Intermittent turbulence in self-similar cascades: divergence of high moments and dimension of the carrier. *J. Fluid Mech.* **62**, 331–358.

MANDELBROT, B. B. 1982 *The Fractal Geometry of Nature*. W. H. Freeman and Company, New York.

MENEVEAU, C. & SREENIVASAN, K. R. 1991 The multifractal nature of turbulent energy dissipation. *J. Fluid Mech.* **224**, 429–484.

MILLER, P. L. & DIMOTAKIS, P. E. 1991 Stochastic geometric properties of scalar interfaces in turbulent jets. *Phys. Fluids* A **3**, 168–177.

PRASAD, R. R., MENEVEAU, C. & SREENIVASAN, K. R. 1988 The multifractal nature of the dissipation field of passive scalars in fully turbulent flows. *Phys. Rev. Lett.* **61**, 74–77.

PRASAD, R. R. & SREENIVASAN, K. R. 1990 The measurement and interpretation of fractal dimensions of the scalar interface in turbulent flows. *Phys. Fluids* A **2**, 792–807.

PRESS, W. H., TEUKOLSKY, S. A., VETTERLING, W. T. & FLANNERY, B. P. 1992 *Numerical Recipes in FORTRAN: The Art of Scientific Computing*. Cambridge University Press, Cambridge.

RICHARDSON, S. F. 1920 The supply of energy from and to atmospheric eddies. *Proc. R. Soc. Lond.* A **97**, 354–373.

SOUTHERLAND, K. B. & DAHM, W. J. A. 1994 A four-dimensional experimental study of conserved scalar mixing in turbulent flows. *Rep.* 026779-12. Department of Aerospace Engineering, The University of Michigan.

SOUTHERLAND, K. B., DAHM, W. J. A. & DOWLING, D. R. 1995 Experimental results for the high wavenumber spectral structure of scalar mixing in turbulent shear flows. In *Proc. 10th Symp. Turbulent Shear Flows*. Pennsylvania State University, University Park, PA.

SREENIVASAN, K. R. 1991 Fractals and multifractals in fluid turbulence. *Ann. Rev. Fluid Mech.* **23**, 539–600.

SREENIVASAN, K. R. & MENEVEAU, C. 1986 The fractal facets of turbulence. *J. Fluid Mech.* **173**, 357–386.

SREENIVASAN, K. R. & PRASAD, R. R. 1989 New results on the fractal and multifractal structure of the large Schmidt number passive scalars in fully turbulent flows. *Physica* D **38**, 322–329.

SREENIVASAN, K. R., RAMSHANKAR, R. & MENEVEAU, C. 1989 Mixing, entrainment and fractal dimension of surfaces in turbulent flows. *Proc. R. Soc. Lond.* A **421**, 79–108.

TAYLOR, G. I. 1935 Statistical theory of turbulence. *Proc. R. Soc. Lond.* A **151**, 421–478.

THEILER, J. 1990 Estimating fractal dimension. *J. Opt. Soc. Am.* A **7**, 1055–1073.